

A Nuclear Structure Model for Double Charge-Exchange Processes

V. dos S. Ferreira¹, A. R. Samana², F. Krmpotić³, and M. Chiapparini¹

¹*Instituto de Física, Universidade do Estado do Rio de Janeiro, CEP 20550-900, Rio de Janeiro-RJ, Brazil*

²*Departamento de Ciências Exatas e Tecnológicas,*

Universidade Estadual de Santa Cruz, CEP 45662-000 Ilhéus, Bahia-BA, Brazil and

³*Instituto de Física La Plata, CONICET, Universidad Nacional de La Plata, 1900 La Plata, Argentina.*

A new model, based on the BCS approach, is specially designed to describe nuclear phenomena $(A, Z) \rightarrow (A, Z \pm 2)$ of double-charge exchange (DCE). After being proposed, and applied in the particle-hole limit, by one of the authors (F. Krmpotić [1]), so far it was never been applied within the BCS mean-field framework, nor has its ability to describe DCE processes been thoroughly explored. It is a natural extension of the pn-QRPA model, developed by Halbleib and Sorensen [2] to describe the single β -decays $(A, Z) \rightarrow (A, Z \pm 1)$, to the DCE processes. As such, it exhibits several advantages over the pn-QRPA model when is used in the evaluation of the double beta decay (DBD) rates. For instance, i) the extreme sensitivity of the nuclear matrix elements (NMEs) on the model parametrization does not occur, ii) it allows to study NMEs, not only for the fundamental state in daughter nuclei, as the pn-QRPA model does, but also for all final 0^+ and 2^+ states, accounting at the same time their excitation energies and the corresponding DBD Q-values, iii) together with the DBD-NMEs it provides also the energy spectra of Fermi and Gamow-Teller DCE transition strengths, as well as the locations of the corresponding resonances and their sum rules, iv) the latter are relevant for both the DBD and the DCE reactions, since the involved nuclear structure is the same; this correlation does not exist within the pn-QRPA model. As an example, detailed numerical calculations are presented for the $(A, Z) \rightarrow (A, Z + 2)$ process in $^{48}\text{Ca} \rightarrow ^{48}\text{Ti}$ and the $(A, Z) \rightarrow (A, Z - 2)$ process in $^{96}\text{Ru} \rightarrow ^{96}\text{Mo}$, involving all final 0^+ states and 2^+ states.

I. INTRODUCTION

The Double Charge-Exchange (DCE) processes relate the (A, Z) nuclei with the $(A, Z + 2)$ and $(A, Z - 2)$ nuclei and will be labeled as $\{+2\}$ and $\{-2\}$ processes respectively.

The most studied DCE process is the Double Beta Decay (DBD). It is the slowest physical process observed so far, and can be used to learn about neutrino physics, provided we know how to deal with the nuclear structure. According with the number and type of leptons we may have the following DBD modes: i) double-electron decay ($2\beta^-$), ii) double-positron decay, iii) electron capture-positron emitting decay ($e\beta^+$), and vi) double electron capture decay (ee). Each of these decays occurs either with the emission of two neutrinos (2ν -decay) or they are neutrinoless (0ν -decay). To simplify the notation and when it does not cause confusion, we will designate the first process as DBD^- and the remaining three as DBD^+ .

The 0ν -decay rates depend on several unknown parameters such as neutrino mass, Majoron coupling, the coupling constants of the right-handed components of the weak hamiltonian, etc.) and the only way to put these in evidence is by having sufficient command over the nuclear structure. It is precisely at this point that the $2\nu 2\beta^\mp$, $2\nu e\beta^+$, and $2\nu ee$ decay modes are important. A comparison between experiment and theory for them provides a measure of the confidence that one may have in the nuclear wave functions employed for extracting the unknown parameters from 0ν -lifetime measurements.

The number of possible candidates for $2\beta^-$ -decay is quite large: there are 35 nuclei. In addition, 34 nuclei can undergo $2e$ -electron capture, while 22 and 6 nuclei

can undergo $e\beta^+$ and $2\beta^+$ -decays respectively [3]. The discovery of the massiveness of the neutrino, through the observation of oscillations, boosted the importance of the 0ν -DBD, since they are the only observables capable of providing the magnitude of the effective neutrino mass.

It is well known that the involved nuclear structure in 2ν and 0ν -DBD is the same one that describes the DCE reactions. This fact reignited recently the interest in the measurements of heavy-ion-induced DCE reactions, such as the NUMEN project [4, 5] involving the $^{40}\text{Ca}(^{18}\text{O}, ^{18}\text{Ne})^{40}\text{Ar}$ process. Simultaneously, the interest in the theoretical study of the DCE reactions has been renewed [6, 7]. More, Shimizu, Menéndez, and Yako [8] have also latterly noted correlations between the DCE and $0\nu 2\beta^-$ -decay. In all the mentioned theoretical studies, the calculations were made within the framework of the shell model (SM).

The neutrinoless DBDs occur in medium-mass nuclei that are often far from closed shells and, as a consequence, the calculations are mostly made in the proton-neutron Quasiparticle Random Phase Approximation (pn-QRPA), since this tool is computationally much more simple than the SM. As discussed in Ref. [9], the kind of correlations that these two methods include are not the same. The pn-QRPA deals with a large fraction of nucleons in a large single-particle space, but within a modest configuration space. The SM, by contrast, deals with a small fraction of nucleons in a limited single-particle space, but allows them to correlate in arbitrary ways within a large configuration space. There is another important difference. The standard pn-QRPA only allows us to calculate the double-charge exchange transitions from the ground state of the decaying (A, Z)

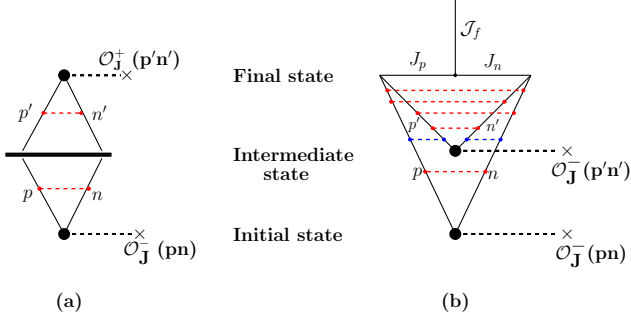


FIG. 1: (Color online) Graphical representation of the numerators in the $2\beta^-$ NME, where the black points indicate the single β -decays. They are: a) $\langle 0_f^+ | \mathcal{O}_J^+ | J_\alpha^+ \rangle \langle J_\alpha^+ | J_{\alpha'}^+ \rangle \langle J_{\alpha'}^+ | \mathcal{O}_J^- | 0_i^+ \rangle$ in the pn-QRPA model, where the overlap between the initial and final QRPA solutions for the intermediate nucleus, $\langle J_\alpha^+ | J_{\alpha'}^+ \rangle$, is represented by a thick line, and b) $\langle \mathcal{J}_f^+ | \mathcal{O}_J^- | J_\alpha^+ \rangle \langle J_\alpha^+ | \mathcal{O}_J^- | 0_i^+ \rangle$ in the (pn,2p2n)-QTDA model, which appears in Eqs. (2.9) and (2.15), and indicates that the first β^- -decay is switched on in the initial state and the second in the intermediate state. The $2\beta^+$ NMEs are represented in the same way after making the substitution $\mathcal{O}_J^+ \leftrightarrow \mathcal{O}_J^-$. The pn, and nn + pp nuclear interactions between protons and neutrons are indicated by red and blue dashed lines, respectively. The five vertices of the diagram b) correspond to five of six angular momentum coupling in the symbol 9j in Eq. (2.47). The sixth coupling $(JJ)\mathcal{J}$ corresponds to the three unconnected lines in this figure.

nucleus to the ground state in the final $(A, Z \pm 2)$ nuclei. In fact, to evaluate the transitions going to the excited states, a second (pp + nn)-QRPA must be performed [10, 11], which introduces additional free parameters and it is limited to one and two quadrupole phonon states.

To deal with the DCE processes we will resort here to a Tamm-Dancoff Approximation (TDA), which has been suggested and discussed on its ph -limit for ^{48}Ca more than a decade ago in Ref. [1]. In this model is assumed that the initial, intermediate and final nuclei are the BCS vacuum, pn-excitations, and 2p2n-excitations respectively. The resulting model will be labeled as (pn,2p2n)-QTDA. The main differences with the standard pn-QRPA model are illustrated in Fig. 1.

The present model is a natural extension to double charge-exchange processes of the pn-QRPA model, originally proposed by Halbleib and Sorensen (HS) in 1967 to describe the single β -decays [2]. As such, it allows to evaluate the NME, not only for the ground states but also of all final 0^+ and 2^+ states, as well as the Q -values for the $2\beta^-$ -decay ($Q_{2\beta^-}$), and for the $2e$ -capture (Q_{2e}). It yields as well the DCE energy strength spectra and their sum rules, which are relevant for associated reaction processes and resonances. Detailed numerical calculations are performed in the present work for the $^{48}\text{Ca} \rightarrow ^{48}\text{Ti}$, and $^{96}\text{Ru} \rightarrow ^{96}\text{Mo}$ processes, involving their final 0^+ and

2^+ states.

II. FORMALISM

A. Nuclear matrix elements and double charge-exchange excitations

Independently of the nuclear model used, and when are only considered the allowed transitions, *i.e.* the Gamow-Teller (GT) and Fermi (F) transitions, the NMEs for the $2\nu 2\beta^\pm$ -decay, from the ground state 0_i^+ in the initial nucleus (A, Z) to one of the states 0_f^+ in the final nuclei $(A, Z \mp 2)$, reads ¹

$$M^{2\nu^\pm}(0_f^+) = M_F^{2\nu^\pm}(0_f^+) + M_{GT}^{2\nu^\pm}(0_f^+) \quad (2.1)$$

$$\equiv \sum_{J=0,1} (-)^J g_J^2 \sum_{\alpha} \left[\frac{\langle 0_f^+ | \mathcal{O}_J^\pm | J_\alpha^\pm \rangle \langle J_\alpha^\pm | \mathcal{O}_J^\pm | 0_i^+ \rangle}{\mathcal{D}_{J_\alpha, 0_f}^{2\nu^\pm}} \right],$$

where $g_0 \equiv g_V$ and $g_1 \equiv g_A$ are the vector and axial-vector weak coupling constants respectively, and the summation goes over all intermediate virtual states $|J_\alpha^\pm\rangle$ in the nuclei $(A, Z \mp 1)$.

The one-body operators are

$$\mathcal{O}_J^- = \hat{J}^{-1} \sum_{pn} \langle p | \mathcal{O}_J | n \rangle (c_p^\dagger c_{\bar{n}})_J,$$

$$\mathcal{O}_J^+ = \hat{J}^{-1} \sum_{pn} \langle n | \mathcal{O}_J | p \rangle (c_n^\dagger c_{\bar{p}})_J, \quad (2.2)$$

with $\mathcal{O}_0 = 1$, and $\mathcal{O}_1 = \sigma$ for F and GT transitions, respectively, and $c_k^\dagger \equiv c_{j_k, m_k}^\dagger$ and $c_{\bar{k}} \equiv (-)^{j_k - m_k} c_{j_k, -m_k}$ being the single-particle creation and annihilation operators, and $\hat{J} = \sqrt{2J+1}$.

The energy denominator in (2.1) is ²

$$\mathcal{D}_{J_\alpha, \mathcal{J}_f}^{2\nu^\pm} = E_{J_\alpha}^{\{\mp 1\}} - \frac{E_{0^+}^{\{0\}} + E_{\mathcal{J}_f}^{\{\mp 2\}}}{2}$$

$$= E_{J_\alpha}^{\{\mp 1\}} - E_{0^+}^{\{0\}} + \frac{E_{0^+}^{\{0\}} - E_{\mathcal{J}_f}^{\{\mp 2\}}}{2}, \quad (2.3)$$

where $E_{0^+}^{\{0\}}$, $E_{J_\alpha}^{\{\pm 1\}}$ and $E_{\mathcal{J}_f}^{\{\pm 2\}}$ are the energies of the decaying (A, Z) nucleus in its ground state, the interme-

¹ For the first-forbidden NME see Ref. [12].

² The last term in the denominator (2.3) is based on the assumption that the lepton energies can be replaced by $e + \nu \cong (E_{0^+}^{\{0\}} - E_{\mathcal{J}_f}^{\{\mp 2\}})/2$, whose validity for the mixed mode was questioned by Hirsch et. al [50]. Following their idea on equal sharing of the liberated energy among the emitted leptons, Suhonen [10] has derived formulas for the three different DBD⁺, and has used them in the evaluation of the decay $^{96}\text{Ru} \rightarrow ^{96}\text{Mo}$. Unfortunately, the author has omitted a factor of 2 in his Eq.(13), which makes wrong the numerical result of mode $2\beta^+$. The same error was propagated in subsequent works [14, 15]. Here we will continue using the estimate (2.3).

diate ($A, Z \pm 1$) nuclei in the state J_α^+ , and final ($A, Z \pm 2$) nuclei in the state \mathcal{J}_f^+ , respectively.

The matrix elements $\langle J_\alpha^+ || \mathcal{O}_J^\pm || 0_i^+ \rangle$ can be expressed as a product of model dependent one-body densities

$$\begin{aligned}\rho^-(pnJ_\alpha) &= \hat{J}^{-1} \langle J_\alpha || (c_p^\dagger c_{\bar{n}})_J || 0_i^+ \rangle, \\ \rho^+(pnJ_\alpha) &= \hat{J}^{-1} \langle J_\alpha || (c_n^\dagger c_{\bar{p}})_J || 0_i^+ \rangle,\end{aligned}\quad (2.4)$$

and a purely geometric (angular) factors³

$$\begin{aligned}O_J(pn) &\equiv \langle p || O_J || n \rangle \\ &= \delta_{l_p l_n} \sqrt{2} \hat{J}_n \hat{J}_p (-)^{j_p + l_p + J + \frac{1}{2}} \begin{Bmatrix} j_p & j_n & J \\ \frac{1}{2} & \frac{1}{2} & l_n \end{Bmatrix},\end{aligned}\quad (2.5)$$

which is the single-particle NME, with $O_J(np) = (-)^{j_n - j_p} O_J(pn)$. Namely,

$$\langle J_\alpha^+ || \mathcal{O}_J^\pm || 0_i^+ \rangle = \sum_{pn} \rho^\pm(pnJ_\alpha^\pi) O_J(pn). \quad (2.6)$$

Similarly,

$$\langle \mathcal{J}_f^+ || \mathcal{O}_J^\pm || J_\alpha^+ \rangle = \sum_{np} \rho^\pm(pnJ_\alpha, \mathcal{J}_f^+) O_J(pn), \quad (2.7)$$

where

$$\begin{aligned}\rho^+(pnJ_\alpha, \mathcal{J}_f^+) &= \hat{J}^{-1} \langle \mathcal{J}_f^+ || (c_n^\dagger c_{\bar{p}})_J || J_\alpha \rangle, \\ \rho^-(pnJ_\alpha, \mathcal{J}_f^+) &= \hat{J}^{-1} \langle \mathcal{J}_f^+ || (c_p^\dagger c_{\bar{n}})_J || J_\alpha \rangle,\end{aligned}\quad (2.8)$$

are the corresponding density matrices for transitions from the intermediate states $|J_\alpha\rangle$ to the final states $|\mathcal{J}_f^+\rangle$, with $\mathcal{J} = 0, 2$.

The corresponding matrix elements are:

$$\begin{aligned}M_F^{2\nu^\pm}(0_f^+) &= g_V^2 \sum_\alpha \frac{\langle 0_f^+ || \mathcal{O}_0^\pm || 0_\alpha^+ \rangle \langle 0_\alpha^+ || \mathcal{O}_0^\pm || 0_i^+ \rangle}{\mathcal{D}_{0_\alpha^+, 0_f^+}^{2\nu^\pm}}, \\ M_{GT}^{2\nu^\pm}(\mathcal{J}_f^+) &= \frac{-g_A^2}{\sqrt{\mathcal{J}+1}} \sum_\alpha \frac{\langle \mathcal{J}_f^+ || \mathcal{O}_1^\pm || 1_\alpha^+ \rangle \langle 1_\alpha^+ || \mathcal{O}_1^\pm || 0_i^+ \rangle}{\left(\mathcal{D}_{1_\alpha^+, \mathcal{J}_f^+}^{2\nu^\pm} \right)^{\mathcal{J}+1}},\end{aligned}\quad (2.9)$$

where the GT-NMEs to 2_f^+ states have also been included [16–18].

All the information about the nuclear structure is contained in the one-body density matrices (2.4) and (2.8), or more precisely in the two-body density matrices

$$\rho^\pm(pnp'n'; J_\alpha, \mathcal{J}_f^+) = \rho^\pm(pn; J_\alpha) \rho^\pm(p'n'; J_\alpha, \mathcal{J}_f^+). \quad (2.10)$$

The NME for the $0\nu 2\beta^\pm$ -decays to the 0_f^+ final states can be easily evaluated from these densities. In fact, after doing in [19, Eqs. (2.20)] the replacement

$$\rho^{ph}(pnp'n'; J_\alpha) \rightarrow \rho^\pm(pnp'n'; J_\alpha, 0_f^+), \quad (2.11)$$

we can express them as

$$M^{0\nu^\pm}(0_f^+) = \sum_X M_X^{0\nu^\pm}(0_f^+), \quad (2.12)$$

where $X = V, A, P, M$ stands for vector (V), axial-vector (A), pseudo-scalar (P), and weak-magnetism (M) terms. We proceed in the same way with the NME $M^{0\nu^\pm}(2_f^+)$.

It is well known that the single β -decay processes to the states J_α in ($A, Z+1$) and ($A, Z-1$) nuclei are related to the following single charge-exchange transition strengths

$$S_J^{\{\pm 1\}} \equiv \sum_\alpha B_{J_\alpha}^{\{\pm 1\}} = \hat{J}^{-2} \sum_\alpha |\langle J_\alpha^+ || \mathcal{O}_J^\mp || 0_i^+ \rangle|^2. \quad (2.13)$$

When $|J_\alpha^+\rangle$ is a complete set of excited states that can be reached by operating with \mathcal{O}_J^\pm on the initial state $|0_i^+\rangle$, they satisfy the single-charge exchange (SCE) sum rule or Ikeda sum rule, for both the F and GT transitions,

$$\begin{aligned}S_J^{\{1\}} &\equiv S_J^{\{+1\}} - S_J^{\{-1\}} \\ &= (-)^J \hat{J}^{-2} \langle 0_i^+ || [\mathcal{O}_J^+, \mathcal{O}_J^-]_0 || 0_i^+ \rangle = N - Z.\end{aligned}\quad (2.14)$$

Similarly, both $M^{2\nu 2\beta^\pm}(\mathcal{J}_f^+)$ and $M^{0\nu 2\beta^\pm}(\mathcal{J}_f^+)$ are related to the double-charge-exchange operators $(\mathcal{O}_J^\pm \mathcal{O}_J^\pm)_\mathcal{J}$ and to their spectral distributions in nuclei ($A, Z \pm 2$) nuclei given by

$$\begin{aligned}S_{J\mathcal{J}}^{\{\pm 2\}} &\equiv \sum_f B_{J\mathcal{J}_f}^{\{\pm 2\}} \\ &= \hat{J}^{-2} \sum_f \left| \sum_\alpha \langle \mathcal{J}_f^+ || \mathcal{O}_J^\mp || J_\alpha^+ \rangle \langle J_\alpha^+ || \mathcal{O}_J^\mp || 0_i^+ \rangle \right|^2.\end{aligned}\quad (2.15)$$

When both $|J_\alpha^+\rangle$ and $|\mathcal{J}_f^+\rangle$ are complete set of excited states that can be reached by operating with \mathcal{O}_J^\pm , and $(\mathcal{O}_J^\pm \mathcal{O}_J^\pm)_\mathcal{J}$ on the initial state $|0_i^+\rangle$, their differences

$$\begin{aligned}S_{J\mathcal{J}}^{\{2\}} &= S_{J\mathcal{J}}^{\{+2\}} - S_{J\mathcal{J}}^{\{-2\}} \\ &= \hat{J}^{-2} \sum_f \left[\left| \sum_\alpha \langle \mathcal{J}_f^+ || \mathcal{O}_J^- || J_\alpha^+ \rangle \langle J_\alpha^+ || \mathcal{O}_J^- || 0_i^+ \rangle \right|^2 \right. \\ &\quad \left. - \left| \sum_\alpha \langle \mathcal{J}_f^+ || \mathcal{O}_J^+ || J_\alpha^+ \rangle \langle J_\alpha^+ || \mathcal{O}_J^+ || 0_i^+ \rangle \right|^2 \right]\end{aligned}\quad (2.16)$$

obey the double-charge-exchange sum rules (DCESR), which were evaluated in Refs. [6, 7, 20–22] with the following results:

$$S_{DF} \equiv S_{00}^{\{2\}} = 2(N - Z)(N - Z - 1), \quad (2.17)$$

³ We use here the angular momentum coupling scheme $|(\frac{1}{2}, l) j \rangle$.

$$S_{DGT,0} \equiv S_{10}^{\{2\}} \quad (2.18)$$

$$= 2(N-Z) \left(N-Z+1+2S_1^{\{+1\}} \right) - \frac{2}{3}C,$$

$$S_{DGT,2} \equiv S_{12}^{\{2\}} \quad (2.19)$$

$$= 10(N-Z) \left(N-Z-2+2S_1^{\{+1\}} \right) + \frac{5}{3}C,$$

where C is a relatively small quantity given by [21, Eq. (4)]. These equations agree with the Eq. (8) in Ref. [7] except for a factor of 3 and the omission of $S_1^{\{+1\}}$.

Combining Eqs. (2.18) and (2.19) one obtains the sum rule for the total GT strength

$$S_{DGT} = 12(N-Z) \left(N-Z-\frac{3}{2}+2S_1^{\{+1\}} \right) + C, \quad (2.20)$$

which is independent of the structure of the ground-state wave function [21].

The relationship between the $\beta\beta$ -decay and double charge exchange reactions has been discussed recently in Refs. [4, 8].

B. (pn,2p2n)-QTDA Model

The pn-QRPA evaluations of the $\beta\beta$ -decays are generally limited to the ground state of the final nuclei, *i.e.* to the calculation of $M_{2\nu}(0_1^+)$ and $M_{0\nu}(0_1^+)$. Moreover, the SCE sum rules (2.14) are fulfilled within this model, but it does not allow us to evaluate the strengths $S_{J\mathcal{J}}^{\beta\beta\pm}$ given by (2.16) and to discuss the corresponding DCESR listed in Eqs. (2.17)-(2.20).

To describe the intermediate states J_α^+ in both pn-QRPA and (pn,2p2n)-QTDA models it is used a nuclear Hamiltonian of the type

$$H_1 = H_0 + H_{pn}, \quad (2.21)$$

where

$$H_0 = \sum_{\alpha} E_k a_k^\dagger a_k \quad (2.22)$$

is the independent-quasiparticle Hamiltonian, with a_α^\dagger and a_α being the single-quasiparticle creation and annihilation operators, defined by the Bogoljubov transformation [23, Eqs. (13.10)]

$$\begin{aligned} a_k^\dagger &= u_a c_k^\dagger + v_k c_{\bar{k}}, \\ a_{\bar{k}} &= u_a c_{\bar{k}} - v_a c_k^\dagger. \end{aligned} \quad (2.23)$$

The proton and neutron pairing interactions are contained in the transformation coefficients u_a and v_a , and in the quasiparticle energy

$$E_k = [(e_k - \lambda)^2 + \Delta_k^2]^{\frac{1}{2}}, \quad (2.24)$$

where e_k is the shell-model single-particle energy (spe), and λ is the chemical potential or Fermi level. The energy gap parameters Δ_k and the pairing coupling constants are determined to reproduce the experimental odd-mass difference for each nucleus. Finally, H_{pn} is the quasiproton-quasineutron interaction.

Within the pn-QRPA, the states $|J_\alpha\rangle$ with excitation energy ω_{J_α} , are created from the correlated initial and final 0^+ ground states by proton-neutron phonon creation operators Q_{J_α} , which are defined as a linear superposition of creation and annihilation proton-neutron quasiparticle pair operators

$$A^\dagger(pnJ) = [a_p^\dagger a_n^\dagger]_J, \quad (2.25)$$

that is

$$\begin{aligned} |J_\alpha\rangle &= Q_{J_\alpha}^\dagger |0^+\rangle \\ &\equiv \sum_{pn} [X_{pnJ}^\alpha A^\dagger(pnJ) - Y_{pnJ}^\alpha A(pnJ)] |0^+\rangle, \end{aligned} \quad (2.26)$$

and

$$Q_{J_\alpha} |0^+\rangle = 0, \quad H_1 |J_\alpha\rangle = \omega_{J_\alpha} |J_\alpha\rangle. \quad (2.27)$$

Usually this is done for initial $|0_I^+\rangle$ and final $|0_F^+\rangle$ ground states, obtaining two sets of intermediate states J_α and $J_{\alpha'}$ in the $(N-1, Z+1)$ nucleus, which are different from each other. Therefore, in the evaluation of the $\beta\beta$ -NME it is necessary to consider their overlap, which is indicated in Fig. 1, which corresponds to the substitution

$$\begin{aligned} \sum_{J_\alpha} \rho^{ph}(pn p' n'; J_\alpha) \rightarrow \langle 0_I^+ | 0_F^+ \rangle \times \\ \sum_{J_\alpha J_{\alpha'}} \rho^+(p' n'; J_{\alpha'}) \langle J_{\alpha'} | J_\alpha \rangle \rho^-(pn; J_\alpha). \end{aligned} \quad (2.28)$$

The ground state defined in (2.27) is more accurate than the BCS ground state ($a_k |BCS\rangle = 0$) since it contains terms with $0, 4, 8, \dots$ quasiparticles [9]. Nevertheless, in the present model we approximate the initial ground state in the (A, Z) nucleus by the BCS vacuum and the states $|J_\alpha\rangle$ in the intermediate $(A, Z \mp 1)$ nuclei as

$$\begin{aligned} |J_\alpha\rangle &= \sum_{pn} X_{pnJ_\alpha} A^\dagger(pnJ) |BCS\rangle, \\ H_1 |J_\alpha\rangle &= \omega_{J_\alpha} |J_\alpha\rangle. \end{aligned} \quad (2.29)$$

This disadvantage of the present model is counteracted by the description that we make of the final states in the $(A, Z \mp 2)$ nuclei. That is, instead of the correlated $|0_F^+\rangle$ state defined in (2.26), we have

$$\begin{aligned} |\mathcal{J}_f^+\rangle &= \sum_{p_1 p_2 n_1 n_2 J_n J_p} Y_{p_1 p_2 J_p, n_1 n_2 J_n; \mathcal{J}_f^+} \\ &\times |p_1 p_2 J_p, n_1 n_2 J_n; \mathcal{J}^+\rangle_A, \end{aligned} \quad (2.30)$$

where $\mathcal{J}^+ = 0^+, 2^+$ and

$$\begin{aligned} & |p_1 p_2 J_p, n_1 n_2 J_n; \mathcal{J}^+ \rangle_A \\ &= [\mathcal{A}^\dagger(p_1 p_2 J_p) \mathcal{A}^\dagger(n_1 n_2 J_n)]^{\mathcal{J}^+} |BCS\rangle, \end{aligned} \quad (2.31)$$

are antisymmetrized and normalized two-proton-two-neutron quasiparticle states, with

$$\begin{aligned} \mathcal{A}^\dagger(abJ) &= N(ab) \mathcal{A}^\dagger(abJ), \\ N(ab) &= \frac{1}{\sqrt{1 + \delta_{ab}}}, \end{aligned} \quad (2.32)$$

being normalized two-quasiparticle states.

The amplitudes $Y_{p_1 p_2 J_{12}, n_1 n_2 J'_{12}; \mathcal{J}_f^+}$ are obtained by diagonalizing the Hamiltonian [24, 25]

$$\begin{aligned} H_2 &= H_0 + H_{pn} + H_{nn} + H_{pp}, \\ H_2 |\mathcal{J}_f^+\rangle &= \omega_{\mathcal{J}_f^+} |\mathcal{J}_f^+\rangle, \end{aligned} \quad (2.33)$$

in the basis (2.31) with H_{nn} and H_{pp} being neutron-neutron and proton-proton interactions. Details on the evaluation of matrix elements of H_2 can be found in References [24, 25]. However, our final results are different.

The matrix element of H_{pn} for the odd-odd nucleus reads

$$\begin{aligned} & \langle BCS | A(npJ) H_{pn} A^\dagger(n'p'J) | BCS \rangle \\ &= G(npn'p'J)(u_p u_n u_{p'} u_{n'} + v_p v_n v_{p'} v_{n'}) \\ &+ F(npn'p'J)(u_p v_n u_{p'} v_{n'} + v_p u_n v_{p'} u_{n'}), \end{aligned} \quad (2.34)$$

where the functions G and F are defined in the standard way [26].

The matrix elements of H_{pn} in the basis (2.31) are derived by employing the relation (1A-25) from [27]. We get

$$\begin{aligned} & \langle BCS | [\mathcal{A}^\dagger(n_1 n_2 J_n) \mathcal{A}^\dagger(p_1 p_2 J_p)]^{\mathcal{J}^\dagger} H_{pn} [\mathcal{A}^\dagger(n'_1 n'_2 J'_n) \mathcal{A}^\dagger(p'_1 p'_2 J'_p)]^{\mathcal{J}} | BCS \rangle \\ &= \hat{J}_n \hat{J}_p \hat{J}'_n \hat{J}'_p N(n_1 n_2) N(n'_1 n'_2) N(p_1 p_2) N(p'_1 p'_2) \bar{P}(n_1 n_2 J_n) \bar{P}(p_1 p_2 J_p) \\ &\times \bar{P}(n'_1 n'_2 J'_n) \bar{P}(p'_1 p'_2 J'_p) \sum_{J_1 J_2} \hat{J}_1^2 \hat{J}_2^2 \begin{Bmatrix} n_1 & n_2 & J_n \\ p_1 & p_2 & J_p \\ J_1 & J_2 & \mathcal{J} \end{Bmatrix} \begin{Bmatrix} n'_1 & n'_2 & J'_n \\ p'_1 & p'_2 & J'_p \\ J_1 & J_2 & \mathcal{J} \end{Bmatrix} \\ &\times \langle BCS | \mathcal{A}^\dagger(n_1 p_1 J_1) H_{pn} \mathcal{A}^\dagger(n'_1 p'_1 J_1) | BCS \rangle \delta_{p_2 p'_2} \delta_{n_2 n'_2}, \end{aligned} \quad (2.35)$$

where the operator

$$\bar{P}(p_1 p_2 J) = 1 + (-)^{p_1 - p_2 + J} P(p_1 \leftrightarrow p_2), \quad (2.36)$$

exchanges the particles p_1 and p_2 .

Finally, the matrix element of the neutron-neutron Hamiltonian H_{nn} in the same basis is

$$\begin{aligned} & \langle BCS | [\mathcal{A}^\dagger(n_1 n_2 J_n) \mathcal{A}^\dagger(p_1 p_2 J_p)]^{\mathcal{J}^\dagger} H_{nn} [\mathcal{A}^\dagger(n'_1 n'_2 J'_n) \mathcal{A}^\dagger(p'_1 p'_2 J'_p)]^{\mathcal{J}} | BCS \rangle \\ &= \delta_{J_p J'_p} \delta_{J_n J'_n} \delta_{p_1 p'_1} \delta_{p_2 p'_2} \langle BCS | \mathcal{A}^\dagger(n_1 n_2 J_n) H_{nn} \mathcal{A}^\dagger(n'_1 n'_2 J'_n) | BCS \rangle \\ &= \delta_{J_p J'_p} \delta_{J_n J'_n} \delta_{p_1 p'_1} \delta_{p_2 p'_2} N(n_1 n_2) N(n'_1 n'_2) \\ &\times [(u_{n_1} u_{n_2} u_{n'_1} u_{n'_2} + v_{n_1} v_{n_2} v_{n'_1} v_{n'_2}) G(n_1 n_2 n'_1 n'_2 J_n) \\ &+ (u_{n_1} v_{n_2} u_{n'_1} v_{n'_2} + v_{n_1} u_{n_2} v_{n'_1} u_{n'_2}) F(n_1 n_2 n'_1 n'_2 J_n) \\ &- (-1)^{n_1 + n_2 - J_{12}} (u_{n_1} v_{n_2} v_{n'_1} u_{n'_2} + v_{n_1} u_{n_2} u_{n'_1} v_{n'_2}) F(n_2 n_1 n'_1 n'_2 J_n)], \end{aligned} \quad (2.37)$$

and analogously for the proton-proton Hamiltonian H_{pp} .

The energies in the denominator $\mathcal{D}_{J_\alpha, \mathcal{J}_f}^{2\nu^\pm}$, defined by (2.3), are

$$E_{J_\alpha}^{\{\pm 1\}} - E_{0^+}^{\{0\}} = \omega_{J_\alpha} \pm \lambda_p \mp \lambda_n,$$

$$E_{\mathcal{J}_f}^{\{\pm 2\}} - E_{0^+}^{\{0\}} = \omega_{\mathcal{J}_f} \pm 2\lambda_p \mp 2\lambda_n, \quad (2.38)$$

where λ_p and λ_n are the proton and neutron chemical potentials. Therefore, for both $2\beta^+$ and $2\beta^-$ -decays, they

are

$$\mathcal{D}_{J_\alpha, \mathcal{J}_f}^{2\nu^\pm} \equiv \mathcal{D}_{J_\alpha, \mathcal{J}_f}^{2\nu} = \omega_{J_\alpha} - \frac{\omega_{\mathcal{J}_f}}{2}. \quad (2.39)$$

The lowest energies $E_{0_f^+}^{\{\pm 2\}}$ are directly related with the Q -values for the $2\beta^-$ -decay ($Q_{2\beta^-}$) and for the $2e$ -capture (Q_{2e}), defined as⁴

$$\begin{aligned} Q_{2\beta^-} &= \mathcal{M}(Z, A) - \mathcal{M}(Z+2, A), \\ Q_{2e} &= \mathcal{M}(Z, A) - \mathcal{M}(Z-2, A), \end{aligned} \quad (2.40)$$

where the \mathcal{M} 's are the atomic masses. Namely,

$$\begin{aligned} Q_{2\beta^-} &= E_{0_+^+}^{\{0\}} - E_{0_+^+}^{\{+2\}} = -\omega_{0_+^+} - 2(\lambda_p - \lambda_n), \\ Q_{2e} &= E_{0_+^+}^{\{0\}} - E_{0_+^+}^{\{-2\}} = -\omega_{0_+^+} + 2(\lambda_p - \lambda_n). \end{aligned} \quad (2.41)$$

Note that $Q_{2e} - Q_{2\beta^-} = 4(\lambda_p - \lambda_n)$, and $Q_{2e} + Q_{2\beta^-} = -2\omega_{0_+^+}$.

To evaluate the one-body densities (2.4) and (2.8) we make use of [23, Eqs. (15.4)] to get

$$\begin{aligned} (c_p^\dagger c_n)_{\mathcal{J}} &\rightarrow u_n v_p A^\dagger(npJ), \\ (c_n^\dagger c_{\bar{p}})_{\mathcal{J}} &\rightarrow u_p v_n A^\dagger(pnJ), \end{aligned} \quad (2.42)$$

which from (2.2) and (2.5) immediately yields

$$\rho^\pm(pnJ_\alpha) = X_{pnJ_\alpha} \begin{Bmatrix} u_n v_p \\ u_p v_n \end{Bmatrix}, \quad (2.43)$$

and

$$\langle J_\alpha^+ || \mathcal{O}_J^\pm || 0_i^+ \rangle = \sum_{pn} X_{pnJ_\alpha} O_J^\pm(pn), \quad (2.44)$$

with

$$O_J^\pm(pn) = O_J(pn) \begin{Bmatrix} u_n v_p \\ u_p v_n \end{Bmatrix}. \quad (2.45)$$

The derivation of $\langle \mathcal{J}_f^+ || \mathcal{O}_J^\pm || J_\alpha^+ \rangle$ is more laborious and one gets

$$\begin{aligned} \langle \mathcal{J}_f^+ || \mathcal{O}_J^\pm || J_\alpha^+ \rangle &= \hat{J} \hat{\mathcal{J}}_f \sum_{pn p' n' J_p J_n} (-)^{J_p + J_n} \hat{J}_p \hat{J}_n \\ &\times N(nn') N(pp') Y_{pp' J_p, nn' J_n; \mathcal{J}_f^+} \bar{P}(nn' J_n) \bar{P}(pp' J_p) \\ &\times \begin{Bmatrix} p & p' & J_p \\ n & n' & J_n \\ J & J & \mathcal{J} \end{Bmatrix} X_{p' n' J_\alpha} O_J^\pm(pn). \end{aligned} \quad (2.46)$$

⁴ The $2\beta^+$ and β^+e Q -values are:

$$\begin{aligned} Q_{2\beta^+} &= \mathcal{M}(Z, A) - \mathcal{M}(Z-2, A) - 4m_e, \\ Q_{\beta^+e} &= \mathcal{M}(Z, A) - \mathcal{M}(Z-2, A) - 2m_e. \end{aligned}$$

The densities $\rho^\pm(pn; J_\alpha^\pi, \mathcal{J}_f^+)$ result immediately (2.7) and (2.46).

Making use of orthogonality and completeness of both basis $|J_\alpha\rangle$ and $A^\dagger(pnJ)|BCS\rangle$ in (2.29), the relation (2.15) can be expressed in a more compact form. Namely as,

$$\begin{aligned} B_{J\mathcal{J}}^{\{\pm 2\}} &= \hat{J}^2 \left| \sum_{pp' nn' J_p J_n} (-)^{J_p + J_n} \hat{J}_p \hat{J}_n N(nn') N(pp') \right. \\ &\times Y_{pp' J_p, nn' J_n; \mathcal{J}_f^+} \bar{P}(nn' J_n) \bar{P}(pp' J_p) \\ &\times \left. \begin{Bmatrix} p & p' & J_p \\ n & n' & J_n \\ J & J & \mathcal{J} \end{Bmatrix} O_J^\mp(p' n') O_J^\mp(pn) \right|^2. \end{aligned} \quad (2.47)$$

In this way, the transition strength turns out to be independent of the intermediate states.

It is important to emphasize that the permutation operators in the last two equations only act on the right side. The physical meaning of these permutations can be inferred from the diagram (b) in Fig. 1, where is graphically represented the DCE matrix element $\sum_\alpha \langle \mathcal{J}_f^+ || \mathcal{O}_J^\pm || J_\alpha^+ \rangle \langle J_\alpha^+ || \mathcal{O}_J^\pm || 0_i^+ \rangle$. This quantity is used in the evaluation of both the $\beta\beta$ -decay NME (2.9) and the DCE transition strengths (2.15), but the Eq. (2.47) is applicable only in the latter case.

Together with the NME $M^{2\nu^\pm}(\mathcal{J}_f^+)$ given by (2.1) and (2.9) with $M^{2\nu^\pm}(2_f^+) \equiv M_{GT}^{2\nu^\pm}(2_f^+)$, we will also evaluate the half-lives $\tau_{2\nu^\pm}^\alpha(\mathcal{J}_f^+)$ for different $\alpha (= 2\beta^-, 2\beta^+, e\beta^+, 2e)$. This is done from

$$[\tau_{2\nu^\pm}^\alpha(\mathcal{J}_f^+)]^{-1} = g_A^4 \left| M^{2\nu^\pm}(\mathcal{J}_f^+) \right|^2 G_{2\nu}^\alpha(\mathcal{J}_f^+), \quad (2.48)$$

i.e. the product of dimensionless axial vector coupling constant, g_A , common NME, $M^{2\nu^\pm}(\mathcal{J}_f^+)$, given in natural units ($\hbar = m_e = c = 1$), and different leptonic kinematics factors, $G_{2\nu}^\alpha(\mathcal{J}_f^+)$, in yr^{-1} . The last ones can be found in [28, Table II] for several nuclei of interest. (For the most recent computations of phase space factors see Refs. [29, 30].)

The excitation energies in the final nuclei are calculated from

$$\mathcal{E}_f = E_{0_+^+}^{\{+2\}} - E_{0_+^+}^{\{+2\}}. \quad (2.49)$$

It should be noted that, just as in the pn-QRPA model the excitation energies in the $(Z, A \pm 1)$ nuclei are the same, in the current model the excitation energies in the $(Z, A \pm 2)$ nuclei are the same.

Finally, the centroid energies of the DCE transition strengths are defined as

$$\bar{E}_{J\mathcal{J}}^{\{\pm 2\}} = \frac{\sum_f \mathcal{E}_{\mathcal{J}_f^+} B_{J\mathcal{J}_f}^{\{\pm 2\}}}{S_{J\mathcal{J}}^{\{\pm 2\}}}. \quad (2.50)$$

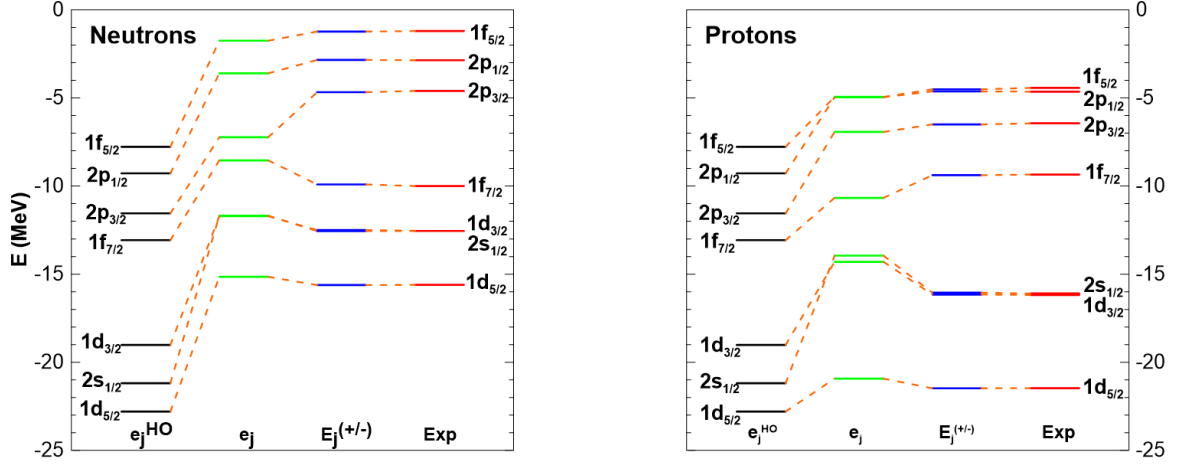


FIG. 2: (Color online) Mean field energies (in units of MeV) for neutrons (left panel) and for protons (right panel). In both cases are shown: (i) harmonic oscillator energies e_j^{HO} , (ii) adjusted single particle energies e_j , (iii) BCS energies relative to the Fermi level ($E_j^{(\pm)}$), and (iv) experimental energies (e_j^{exp}).

III. NUMERICAL RESULTS AND DISCUSSION

The residual interaction is described by the δ -force (in units of $\text{MeV}\cdot\text{fm}^3$)

$$V = -4\pi(v^s P_s + v^t P_t)\delta(r), \quad (3.1)$$

where v^s and v^t are the spin-singlet and spin-triplet parameters.

As usually, the pairing strengths for protons and neutrons, $v_{pair}^s(p)$ and $v_{pair}^s(n)$, are obtained from the fitting of the experimental pairing gaps.

In the numerical evaluations of the matrix elements $G(npn'p'J)$, $F(npn'p'J)$, $G(n_1n_2n'_1n'_2J_n)$, $F(n_1n_2n'_1n'_2J_n)$, $G(p_1p_2p'_1p'_2J_p)$, and $F(p_1p_2p'_1p'_2J_p)$ of the Hamiltonians H_{pn} , H_{pp} , H_{nn} , given by Eqs. (2.32), (2.33) and (2.34), were used the same coupling constants.

To set the coupling constants in the ph -channel we use the energy behavior of the IAS and GTR [31] (see also Refs. [32, 33]), with the results (in units of $\text{MeV}\cdot\text{fm}^3$): i) $v_{ph}^s = 27$ and $v_{ph}^t = 64$ for ^{48}Ca , and ii) $v_{ph}^s = 55$ and $v_{ph}^t = 92$ for all nuclei.

For the coupling constants v_{pp}^s and v_{pp}^t within the pp -channel, we use values close to those obtained in Ref. [19] as a result of the partial restoration of the spin-isospin SU(4) symmetry (PSU4SR). More precisely, this procedure yields $s_{sym} \cong t_{sym} \cong 1$ for the ratios

$$s = \frac{v_{pp}^s}{v_{pair}^s}, \quad t = \frac{v_{pp}^t}{v_{pair}^s}, \quad (3.2)$$

where $\bar{v}_{pair}^s = (v_{pair}^s(p) + v_{pair}^s(n))/2$.⁵

Moreover, instead of using the bare value $g_A = 1.27$ for the axial-vector coupling constant [34], we use an effective value $g_A = 1.0$.⁶ Still smaller values for g_A have been used in the literature [36].

A. Single particle space

The DBD- $^{48}\text{Ca} \rightarrow ^{48}\text{Ti}$ is a rather unique case, since ^{48}Ca is a double closed nuclei, and we can make use of the experimental spe e_j^{exp} . All they were taken from the binding and excitation energies, weighted with spectroscopic factors, of odd-mass neighboring nuclei: ^{47}Ca and ^{49}Ca for neutrons, and ^{47}K and ^{49}Sc for protons. They are listed in Fig. 2 and are those from [38, Table II], except for the proton $f_{5/2}$ spe, which is estimated from the proton $f_{5/2} - f_{7/2}$ splitting given in Ref. [39]. We need this level to saturate both the SCE and DCE sum rules. Once this has been done the spe e_j^{exp} have been used in two different ways:

⁵ Within PSU4SR s and t are determined from the condition that the strengths $S_F^+ \equiv S_0^{\{-1\}}$ and $S_{GT}^+ \equiv S_1^{\{-1\}}$ become minimal (see [19, Fig. 1]).

⁶ This quenching is frequently attributed to the Δ -hole polarization effect on the axial-vector coupling constant [32]. Recently has been presented an explanation of the quenching of g_A within the context of effective field theories [35].

1. The following steps are done in handling the BCS equations [12, 37] :
 - a) The BCS energies relative to the Fermi level λ ,

$$E_j^{(\pm)} = \pm E_j + \lambda, \quad (3.3)$$

are introduced, where the positive (negative) sign is adopted if the corresponding single-particle state is a particle (hole)-state.

b) It is assumed that neutron and proton Fermi levels λ_n , and λ_p lay between $j_n = 2p_{3/2} - 1f_{7/2}$ and $j_p = 1f_{7/2} - 2s_{3/2}$ states respectively, and that all states above λ are pure quasi-particle excitations $E_j^{(+)}$ and all states below λ are pure quasi-hole excitations $E_j^{(-)}$.

c) Starting from a set of harmonic oscillator energies e_j^{HO} , the energies $E_j^{(\pm)}$ are adjusted to the experimental spectra e_j^{exp} by means of a χ^2 search varying the strengths v_s^{pair} and the bare spe e_j which that appear in the BCS gap equations (2.24).

All this procedure is illustrated in Fig. 2.

2. For the sake of completeness the pairing parameters $v_{pair}^s(p)$ and $v_{pair}^s(n)$ were fixed in the standard manner [49]. That is, by fitting the experimental pairing gaps to the calculated pairing gaps Δ_j , given by [27, Eq. (2.96)], with $j = 1f_{7/2}$ for neutrons and $j = 2s_{1/2}$ for protons.

The most relevant difference between the spe e_j^{exp} and e_j is the disappearance of the energy gap between the holes and the particles in the last case. The resulting parameters v_s^{pair} , and λ are given in the Table I for the two sets of spe e_j and e_j^{exp} . The quasiparticle energies $E_j^{(\pm)}$ with e_j^{exp} are obviously slightly different from those shown in Fig. 2.

TABLE I: Results for the BCS coupling constants and Fermi levels. All notation is explained in the text. The λ 's are given in units of MeV, and the couplings v_s^{pair} is in units of MeV·fm³.

Nuclei	spe	$v_s^{pair}(n)$	$v_s^{pair}(p)$	λ_n	λ_p
⁴⁸ Ca	e_j^{exp}	31.45	34.77	-6.587	-13.000
	e_j	25.20	28.35	-7.091	-12.702
⁹⁶ Ru		33.20	38.91	-8.412	-5.663

In the ⁹⁶Ru nucleus, the neutron and proton shells are both open and its energy spectra is clearly rotational. This fact gives rise to a strong interplay between collective and single-particle degrees of freedom in the low energy spectra of the neighboring odd-mass nuclei ⁹⁵Ru, ⁹⁷Ru, ⁹⁵Tc, and ⁹⁷Tc. For instance, it is very likely that the ground state $5/2^+$ in ⁹⁵Ru is a consequence of the $j-1$ anomaly in the three neutron cluster $(1g_{7/2})^3$ [45, 46].

Such a complex nuclear structure inhibits us to determine the appropriate spe spectra and the pairing interaction strengths from experimental energy spectra, as it was done in the case of ⁴⁸Ca.

TABLE II: Neutron and proton spe for ⁹⁶Ru, which were obtained in the way explained in the text, together with the resulting quasiparticle energies (3.3). All notation is explained in the text. The energies are given in units of MeV, and the couplings in units of MeV·fm³.

level	Neutrons		Protons	
	e_j	$E_j^{(\pm)}$	e_j	$E_j^{(\pm)}$
$3s_{1/2}$	-5.396	-5.1817	4.916	5.006
$2d_{3/2}$	-5.236	-4.9834	4.792	4.897
$1g_{7/2}$	-6.878	-6.5267	2.308	2.502
$2d_{5/2}$	-7.401	-10.0514	2.493	2.627
$1g_{9/2}$	-14.401	-14.5004	-5.424	-7.448
$2p_{1/2}$	-17.802	-17.9127	-7.718	-8.478
$2p_{3/2}$	-19.389	-19.4838	-9.295	-9.773

We used instead the spe provided by N. Paar [47], which were calculated in the relativistic Hartree-Bogoliubov model, as outlined in Ref. [48]. They are shown in Table II, together with the resulting quasiparticle energies (3.3), which were obtained following procedure 2 in the case of ⁴⁸Ca. This implies to fit the calculated pairing gaps Δ_j , with $j = 1g_{7/2}$ for neutrons and $j = 1g_{9/2}$ for protons, to the experimental ones. The similarity between the spe e_j and the quasiparticle energies $E_j^{(\pm)}$ is remarkable. The corresponding pairing parameters v_s^{pair} and chemical potentials λ are listed in Table I.

It is important to note that in ⁴⁸Ca it is $\lambda_n > \lambda_p$ while in ⁷⁶Ru this difference is $\lambda_n < \lambda_p$. We will soon see that this fact is decisive with respect to the Q -values of DBD. More precisely, this will explain why DBD⁻ occurs in ⁴⁸Ca and DBD⁺ occurs in ⁷⁶Ru.

Our method of calculation is similar in several aspects to that used in the SM in the Refs. [6, 7]. In fact, the illustration of their calculations, made in Fig. 1 of that reference, is also valid in our case. The biggest difference between the two models, in addition to the residual interactions that were used, arises from the size of the configuration spaces of the final states \mathcal{J}_f^+ . We have 664 0^+ states and 2.470 2^+ states, while Auerbach and Bui Minh Loc [7] have, in their evaluation of double charge-exchange GT strength ⁴⁸Ca \rightarrow ⁴⁸Ti, the quantity of 14.177 and 61.953 final states in the fp -space, respectively. In the case of the ⁹⁶Ru \rightarrow ⁹⁶Mo decay, we also have 664 0^+ states, but 2.583 2^+ states.⁷

⁷ See also our Fig. 1, where the difference with the standard pn-

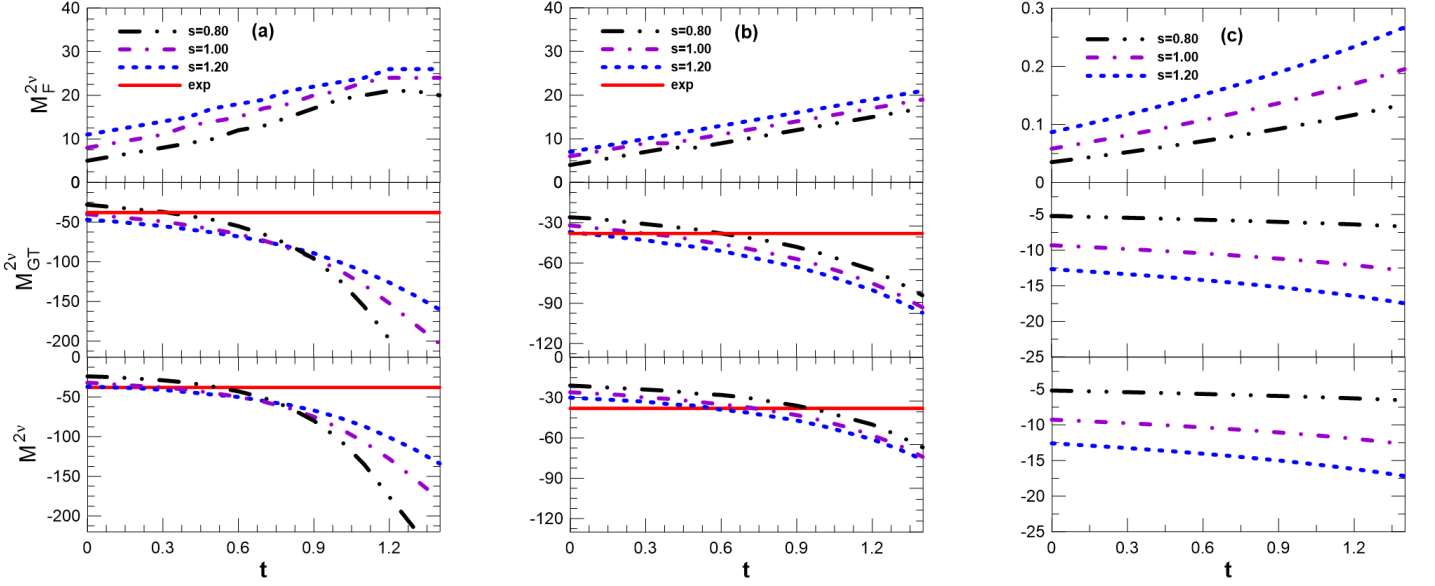


FIG. 3: Calculated NME $M_F^{2\nu}$, $M_{GT}^{2\nu}$ and $M^{2\nu}$ for the ground 0^+ state (in natural units $\times 10^{-3}$), as a function of the pp parameters t and s for ^{48}Ti for: a) ^{48}Ca with spe e_j^{exp} , b) ^{48}Ca with spe e_j , and c) ^{96}Ru . The experimental value for ^{48}Ti $|M^{2\nu}(0_1^+)| = (38 \pm 3) \times 10^{-3}$ is also indicated by the red line, whose width represents the experimental error.

B. Nuclear Matrix Elements

We calculate simultaneously the NMEs $M_F^{2\nu}(0_f^+)$, $M_{GT}^{2\nu}(0_f^+)$, $M^{2\nu}(0_f^+)$, and $M_{GT}^{2\nu}(2_f^+)$ for all above mentioned \mathcal{J}_f^+ final states with the following three sets of pp parameters:

$$\begin{aligned} T1: & \quad s = 0.80, \quad t = 0.80, \\ T2: & \quad s = 0.80, \quad t = 1.00, \\ T3: & \quad s = 1.00, \quad t = 1.00. \end{aligned} \quad (3.4)$$

In the upper part of Table III are shown the results for the $^{48}\text{Ca} \rightarrow ^{48}\text{Ti}$ decays to the ground state 0_1^+ , and the first excited 0_2^+ and 2_1^+ states in ^{48}Ti nucleus, for the two sets of spe e_j listed in Table I. The agreement between the calculated and measured results for $M^{2\nu}(0_1^+)$ can be considered satisfactory (in particular with the spe e_j) in view of the fact that all the nuclear parameters in the pp and ph -channels are so to say fixed, both for identical particles and for different particles. We hope that in the next future the NMEs $M^{2\nu}(0_2^+)$ and $M_{GT}^{2\nu}(2_1^+)$ will also be measured. For both 0^+ levels the F-NME is relatively small compared to the GT one, but in no way it can be neglected. As seen in the Eq. (2.1), these two NMEs always interfere destructively.⁸

The NME $|M^{2\nu}(0_1^+)|$ in ^{48}Ca has been calculated many times, but there are only very few theoretical studies of $M^{2\nu}(0_2^+)$ and $M_{GT}^{2\nu}(2_1^+)$. As far as we know, the first one has been evaluated only in Ref. [41] and the second one in Refs.[17, 41] (see also Ref. [42]). These results, as well as those for NME $|M^{2\nu}(0_1^+)|$, are confronted with our results in Table III. It should be pointed out that in the just mentioned studies have not been considered the contributions of F-NMEs $M_F^{2\nu}(0_{\alpha=1,2}^+)$. Therefore, strictly speaking their results for $|M^{2\nu}(0_{\alpha=1,2}^+)|$ should be compared with ours $|M_{GT}^{2\nu}(0_{\alpha=1,2}^+)|$.

In the lower part of Table III are shown the NMEs for the $^{96}\text{Ru} \rightarrow ^{96}\text{Mo}$ decay to final states $\mathcal{J}^\pi = 0_1^+, 0_2^+$, and 2_1^+ . The results of previous calculations [10, 50–53] are also shown. It is noticeable that the differences between our three calculations are much smaller than the differences with all the other works.

The strong dependence of the NME within the pn-QRPA model with respect to the isoscalar pp parameter t is well known and is often discussed. Therefore, it could be interesting to analyze that dependence in the current model. This is done in Fig. 3 showing the NMEs $M_F^{2\nu}$, $M_{GT}^{2\nu}$ and $M^{2\nu}$ for the ground 0^+ state in ^{48}Ca and ^{96}Ru , as a function of the pp parameters t and s . The experimental value of $|M^{2\nu}(0_1^+)|$ is also drawn. It can be concluded that within the present model such dependence is

⁸ QRPA calculation of the NME is illustrated graphically.

⁸ It is interesting to note that M_F is often omitted in the calcula-

tions, simply invoking isospin conservation.

TABLE III: Calculated and measured NME (in natural units $\times 10^{-3}$) for 2ν -DBDs of ^{48}Ca ($M^{2\nu}(\mathcal{J}_f^+) \equiv M^{2\nu^-}(\mathcal{J}_f^+)$) and ^{96}Ru ($M^{2\nu}(\mathcal{J}_f^+) \equiv M^{2\nu^+}(\mathcal{J}_f^+)$) to ground state 0_1^+ , and first excited 0_2^+ and 2_1^+ states in final nuclei ^{48}Ti and ^{96}Mo , respectively. Results from Refs.[17, 41] for ^{48}Ca and from Refs.[10, 50–53] for ^{96}Ru , as well the experimental value for ^{48}Ca [3], are also shown in same units.

^{48}Ca					
par	$M_F^{2\nu}(0_1^+)$	$M_{GT}^{2\nu}(0_1^+)$	$ M^{2\nu}(0_1^+) $	$ M^{2\nu}(0_2^+) $	$ M^{2\nu}(2_1^+) $
e_j					
T1	11	-44	33	18	0.98
T2	13	-53	40	22	1.08
T3	15	-62	47	15	0.69
e_j^{exp}					
T1	15	-78	63	5.0	0.53
T2	19	-122	103	23	0.60
T3	21	-110	89	34	0.33
[17]			22		120
[41]			28	26	1.62
Exp.			38 ± 3		

^{96}Ru					
T1	0.08	-5.9	5.8	55.6	0.55
T2	0.10	-6.1	6.0	63.6	0.68
T3	0.15	-11.5	11.3	26.8	0.63
[10]			415-1437	492-1554	0.1-8.4
[50]			251		
[51]			101		
[52]			54		
[53]	-0	2170	2170	50	

only moderate. The same statement is valid also for all remaining 2ν NMEs.

It is also well known that the relatively small values of the NME in the pn-QRPA model come from the destructive interference between forward and backward going contributions [19]. That is, trough the ground state correlations (GSC). The quenching mechanism is different in the current model, and it is the consequence of the interplay between seniority-zero and seniority-four configurations in the final states. For example, in the case of ^{48}Ca , within the space e_j and with force parameters T1, the NME $M^{2\nu}$ for the three lowest 0^+ states are: $-0.033, -0.018, -0.043$. While, when only the seniority-zero configurations are considered, one gets: $-0.074, -0.028, -0.090$ respectively, which confirms the above statement.

C. Half-lives

The half-lives are evaluated trivially from (2.47) using the NME and leptonic kinematic factors $G_{2\nu}^\alpha(\mathcal{J}_f^+)$. De-

TABLE IV: Calculated half-lives $\tau_{2\nu}^{2\beta^-}(\mathcal{J}_f^+ = 0_1^+, 0_2^+, 2_1^+)$ in units of yr for the 2ν -DBD $^{48}\text{Ca} \rightarrow ^{48}\text{Ti}$, with spe e_j the pp parameters set and $g_A = 1$ are shown and confronted with previous calculations and experiments. In Eq. (2.47) are used the $G_{2\nu}^\alpha(\mathcal{J}_f^+)$ factors from Ref. [43] for the levels $0_1^+ (= 1.56 \times 10^{-17} \text{ yr}^{-1})$ and $0_2^+ (= 3.63 \times 10^{-22} \text{ yr}^{-1})$, and from Ref. [44] for $2_1^+ (= 4.41 \times 10^{-18} \text{ yr}^{-1})$.

	0_1^+	0_2^+	2_1^+
T1	5.91×10^{19}	8.51×10^{24}	2.36×10^{23}
T2	4.02×10^{19}	5.70×10^{24}	1.94×10^{23}
T3	2.91×10^{19}	1.23×10^{25}	4.76×10^{23}
Ref. [17]			1.72×10^{24}
Ref. [41]	3.3×10^{19}		8.5×10^{23}
Exp [3]	$(4.4^{+0.6}_{-0.5}) \times 10^{19}$		

TABLE V: Calculated half-lives $\tau_{2\nu\pm}^\alpha(0_1^+)$ in units of yr for the 2ν -DBD $^{96}\text{Ru} \rightarrow ^{96}\text{Mo}$, with the pp parameter set T1 and $g_A = 1$ are shown and confronted with previous calculations and experiments. In Eq. (2.47) are used the $G_{2\nu}^\alpha(\mathcal{J}_f^+)$ factors from Ref. [16] for the channels $2\beta^+ (= 1.080 \times 10^{-26} \text{ yr}^{-1})$, $\beta^+e (= 0.454 \times 10^{-21} \text{ yr}^{-1})$, and $ee (= 2.740 \times 10^{-21} \text{ yr}^{-1})$.

α	present	[50]	[51]	[52]	[53]
$2\beta^+$	2.8×10^{30}	5.8×10^{26}		3.485×10^{28}	1.22×10^{16}
β^+e	6.5×10^{25}	1.2×10^{22}	8.6×10^{22}	9.100×10^{23}	3.78×10^{20}
ee	1.1×10^{25}	2.1×10^{21}	1.4×10^{22}	1.628×10^{23}	3.11×10^{17}

spite this, we present some of them only for the sake of completeness.

In Table IV are compared our results for the half-lives $\tau_{2\nu}^{2\beta^-}(\mathcal{J}_f^+ = 0_1^+, 0_2^+, 2_1^+)$ in ^{48}Ca evaluated with spe e_j pp parameters set with the previous ones.

The major difference appears for the 2_1^+ level.

The same is done in Table V for the half-lives $\tau_{2\nu\pm}^\alpha(0_1^+)$ in ^{96}Ru for different channels $\alpha = 2\beta^+, \beta^+e$, and ee . The experimental limits are: $\tau_{2\nu}^{2\beta^+}(0_1^+) \geq 1.4 \times 10^{20} \text{ yr}$ and $\tau_{2\nu}^{\beta^+e}(0_1^+) \geq 0.8 \times 10^{20} \text{ yr}$ [54].

D. Q -values and Energy Spectra

Before starting with the discussion of Q -values, it is convenient to remember that a physical phenomenon is allowed only when this quantity is positive.

In Table VI are confronted the experimental data with our results for the $Q_{\beta\beta}$ and Q_{2e} values in the DCE processes: a) $^{48}\text{Ca} \rightarrow ^{48}\text{Ti}$ and $^{48}\text{Ca} \rightarrow ^{48}\text{Ar}$, and b) $^{96}\text{Ru} \rightarrow ^{96}\text{Mo}$ and $^{96}\text{Ru} \rightarrow ^{96}\text{Pl}$. One sees that the model is capable of reproducing not only the signs of the Q -values, but also their magnitudes, without having to modify the

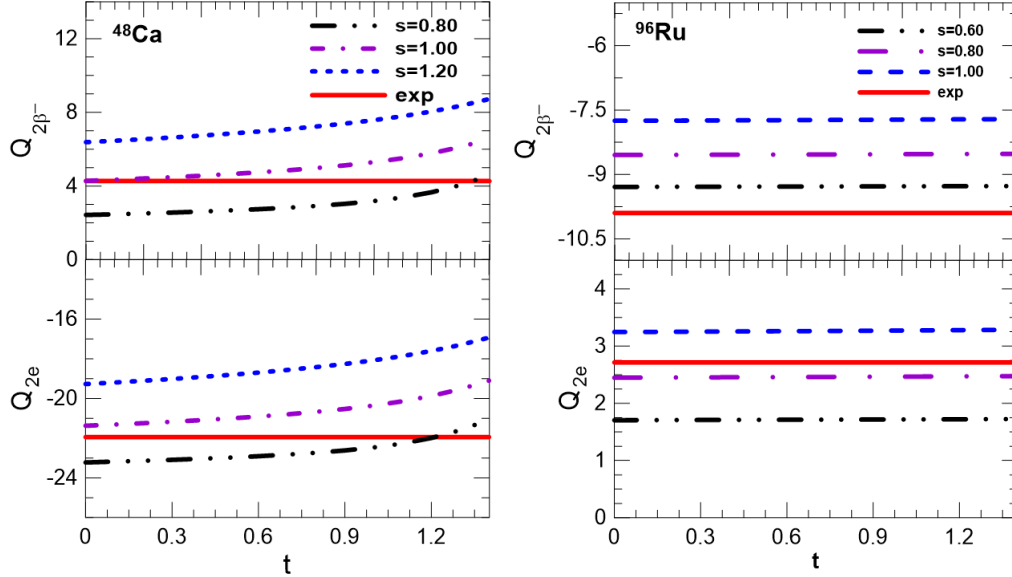


FIG. 4: Calculated $Q_{2\beta^-}$ and Q_{2e} values in ^{48}Ca within the spe space e_j^{exp} (left panel) and ^{96}Ru (right panel), as a function of pp parameters t and s . The experimental Q -values are also shown.

TABLE VI: Calculated $Q_{\beta\beta}$ and Q_{2e} values (in units of MeV) with the three sets of pp parameters T1, T2 and T3 and for the DCE processes: a) $^{48}\text{Ca} \rightarrow ^{48}\text{Ti}$ and $^{48}\text{Ca} \rightarrow ^{48}\text{Ar}$, and b) $^{96}\text{Ru} \rightarrow ^{96}\text{Mo}$ and $^{96}\text{Ru} \rightarrow ^{96}\text{Pl}$, are confronted with the experimental ones.

^{48}Ca			
	par	$Q_{\beta\beta}$	Q_{2e}
e_j^{exp}	T1	2.919	-22.734
	T2	3.185	-22.468
	T3	5.300	-20.353
e_j	T1	5.151	-17.295
	T2	5.232	-17.214
	T3	6.710	-15.736
Exp		4.268	-21.943
^{96}Ru			
e_j	T1	-8.532	2.460
	T2	-8.527	2.465
	T3	-7.721	3.271
Exp		-9.896	2.714

parameters of the model. This is very comforting! In addition, it seems that the model “knows” what type of DCE decay can occur in a given nucleus.

The nature of Q -value is dominantly determined by the proton and neutron pairing mean fields, as seen from (2.41) or, more precisely, from the relation $Q_{2e} - Q_{2\beta^-} =$

$4(\lambda_n - \lambda_p)$. The dependence on the residual interaction is rather weak and takes place through the ground state energy ω_{0+} in residual nuclei, as $Q_{2e} + Q_{2\beta^-} = -2\omega_{0+}$. More details on how the Q -values depend on the pp coupling constants are shown in the Fig. 4.

As we stated before, in the same way that the pn-QRPA model [2] predicts identical energy spectra for odd-odd nuclei ($A, Z \pm 1$), the present model predicts identical excitation energies in even-even nuclei ($A, Z \pm 2$). This is obviously not realistic due to the large neutron excess.

It is pertinent to mention here that the use of particle-number-projection can become very important when working with the BCS mean-field [55]. Without a doubt, through this method different energy spectra are obtained in nuclei for which the number of protons is different.

But, despite the above mentioned handicap, the calculated excitation energies of the 0^+ and 2^+ states in ^{48}Ti are consistent with data, as shown in Fig. 5, where we give the calculated spectra for the two spe spaces and the pp parameterizations T1 and T3. Because of the size of the $Q_{2\beta^-}$ -value ($= 4.268$ MeV), the $2\beta^-$ -decays are energetically possible for all states, except for 0_4^+ . We have evaluated the NMEs for all these states, but we do not consider necessary to present them here. It should also be said that we have not found in the literature any detailed calculation of the ^{48}Ti low energy spectrum to compare with ours. Finally, the ^{96}Mo energy spectrum is not well explained by the current model and, therefore,

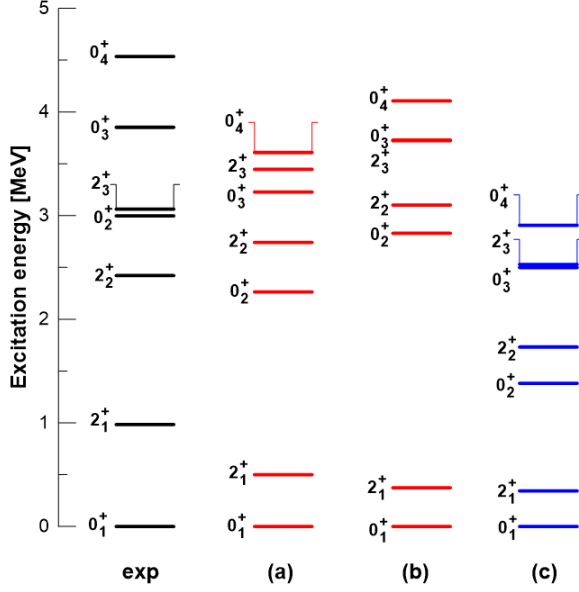


FIG. 5: Measured excitation energies in ^{48}Ti are compared with the calculations: (a) and (b) with the spe e_j^{exp} and pp parametrization T1 and T3 respectively, and (c) with the spe e_j and pp parametrization T1.

will not be discussed here.

E. Double-Charge-Exchange Strengths and their Sum Rules

In Table VII are displayed the results for the DCE transition strengths $S_{J\mathcal{J}}^{\{\pm 2\}}$ given by (2.15), both for Fermi ($J = 0; \mathcal{J} = 0$) and Gamow-Teller ($J = 1; \mathcal{J} = 0, 2$). The corresponding sum rules $S_{J\mathcal{J}}^{\{2\}}$ calculated from (2.16) are also shown, and confronted with the predicted sum rules $S_{J\mathcal{J}}^{\{2\}}$ given by (2.17), (2.18), and (2.19).

In addition, to know the locations of the DCE resonances, we have evaluated the centroid energy (2.46), and to get an idea of the magnitudes of the DBD, the strengths $B_{J\mathcal{J}_1}^{\{+2\}}$ ($B_{J\mathcal{J}_1}^{\{-2\}}$) going to the levels 0_1^+ and 2_1^+ in final ^{48}Ti (^{96}Mo) nucleus are explicitly given.

All calculations related to DCE transition strengths were performed for the three sets of pp parameters (3.4), finding that all produce identical results. We have also found that, at least in the case of ^{48}Ca , there is a certain dependence of the results with respect to the spe spaces used.

In the last three rows of the upper part of the Table VII, are given the results derived for ^{48}Ca by other au-

thors within the SM for the pf -space.⁹ Namely, by i) Sagawa and Uesaka [6] with GXFF1A interaction, and by ii) Auerbach and Minh Loc [7], and Shimizu, Menéndez and Yako [8], both with KB3G interaction. In fact, the values of strengths $S_{1\mathcal{J}=0,2}^{\{+2\}}$ attributed to the last authors [8] have been extracted from their Fig. 1.

TABLE VII: Results with the pp parametrization T1 for: i) Fermi ($J = 0; \mathcal{J} = 0$) and Gamow-Teller ($J = 1; \mathcal{J} = 0, 2$) DCE transition strengths $S_{J\mathcal{J}}^{\{\pm 2\}}$ given by (2.15), ii) the corresponding sum rules $S_{J\mathcal{J}}^{\{2\}}$ calculated from (2.16), iii) the predicted sum rules $S_{J\mathcal{J}}^{\{2\}}$ given by (2.17), (2.18), and (2.19), iv) the energy centroid (2.49), and v) the transition strengths $B_{J\mathcal{J}_1}^{\{2\}}$ ($\equiv B_{J\mathcal{J}_1}^{\{+2\}}$) for ^{48}Ca and $B_{J\mathcal{J}_1}^{\{2\}}$ ($\equiv B_{J\mathcal{J}_1}^{\{-2\}}$) for ^{96}Ru going to the levels 0_1^+ and 2_1^+ . The SM results from previous works [6–8] for ^{48}Ca are also shown. The meaning of the inequalities is explain in the text.

^{48}Ca								
Ref.	$J\mathcal{J}$	$S_{J\mathcal{J}}^{\{-2\}}$	$S_{J\mathcal{J}}^{\{+2\}}$	$S_{J\mathcal{J}}^{\{2\}}$	$S_{J\mathcal{J}}^{\{2\}}$	$\bar{E}_{00}^{\{-2\}}$	$\bar{E}_{00}^{\{+2\}}$	$B_{J\mathcal{J}_1}^{\{2\}} \times 10^{-3}$
e_j^{exp}	00	140.1	0.94	139.1	112	20.5	—	77
	10	162.2	2.0	160.2	≤ 175.9	12.2	15.9	470
	12	716.1	9.10	707.0	≥ 640.0	13.2	16.5	51
e_j	00	157.1	2.38	139.1	112	21.6	22.7	45
	10	189.8	5.87	160.2	≤ 183.9	14.1	19.7	163
	12	858.5	26.1	832.4	≥ 752.5	14.8	19.7	52
[6]	10	—	—	$135.5 \leq 144.0$	—	—	—	—
	12	—	—	$501.2 \geq 480.0$	—	—	—	—
[7]	10	131.8	—	≤ 144.0	—	21.9	—	0.24
[8]	10	126.3	—	—	—	—	—	—
	12	511.0	—	—	—	—	—	—
^{96}Ru								
e_j	00	128.0	0.1	127.9	112	21.4	20.4	0.0016
	10	221.1	12.0	209.1	≤ 222.7	23.1	13.1	16
	12	981.4	49.4	932.0	≥ 873.4	23.1	12.3	5.7

Several observations are in order regarding the results shown in Table VII:

1. The strengths $S_{J\mathcal{J}}^{\{-2\}}$ are always small in comparison with the strengths $S_{J\mathcal{J}}^{\{+2\}}$ and as a consequence $S_{J\mathcal{J}}^{\{+2\}} \cong S_{J\mathcal{J}}^{\{2\}}$. This is clearly due to the relatively large neutron excess.
2. Although small, the strengths $S_{J\mathcal{J}}^{\{-2\}}$ are significant in relation to the DBD. They are proportionally higher in ^{96}Ru , which decays by $\beta^+\beta^+$, than in ^{48}Ca , which decays by $\beta^-\beta^-$.

⁹ Note that the present calculations were done in a single-particle space consisting of the $2p - 1f - 2s - 1d$ shells for both protons and neutrons.

3. The F strengths $S_{00}^{\{2\}}$ deviate quite significantly from the sum rule strengths $S_{00}^{\{2\}}$; 24% and 40%, respectively, within the spe spaces e_j^{exp} and e_j in ^{48}Ca , and 14% in ^{96}Ru . A possible explanation for these differences is given in the appendix.¹⁰
4. Terms proportional to C in the GT sum rules (2.18), (2.19), and (2.20) are not included in the calculations, and this is the reason why have to be fulfilled the conditions

$$\begin{aligned} S_{10}^{\{2\}} &\leq S_{10}^{\{2\}}, \\ S_{12}^{\{2\}} &\geq S_{12}^{\{2\}}. \end{aligned} \quad (3.5)$$

In fact, they are nicely satisfied in all numerical calculations presented in Table VII.

5. All $S_{J\mathcal{J}}^{\{\mp 2\}}$ strengths depend quite significantly on the spe, but very weakly on the residual interaction. This is the reason why we only show the results for the parametrization T1.
6. The same situation applies to the predicted sum rules $S_{1\mathcal{J}}^{\{2\}}$, due to their dependence on the term $S_1^{\{+1\}}$ (in Eqs. (2.18), (2.19) and (2.20)), which in turn depends on the spe used in the calculations.
7. The terms proportional to C are omitted in (2.18), (2.19) in Refs. [6, 7], and this is the reason why their predicted sum rules $S_{1\mathcal{J}}^{\{2\}}$ are smaller than ours.
8. Since the values for $S_{1\mathcal{J}}^{\{+2\}}$ are not explicitly given in Shimizu *et al.* [8], we have derive them from their Fig. 1b. They are consistent with the values of $S_{1\mathcal{J}}^{\{2\}}$ presented in Refs. [6, 7].
9. Our GT strengths are always larger than those in the SM calculations. Also our average energies $\bar{E}_{1\mathcal{J}}^{\{+2\}}$ are significantly smaller that those presented in Table II in Ref. [7], and those shown in Fig. (1b) by Shimizu *et al.* [8]. It is difficult to discern whether this is due to the deficiency of our model, or the difference in the size of single-particle spaces. We are inclined to think that our results are correct, since otherwise it would be very difficult to satisfy the second condition in Eq. (3.5).
10. The size of $B_{J\mathcal{J}_1}^{\{\pm 2\}}$, shown in the last column of Table VII, and when compared with $S_{J\mathcal{J}}^{\{\pm 2\}}$, give us an idea on the smallness of the NMEs.

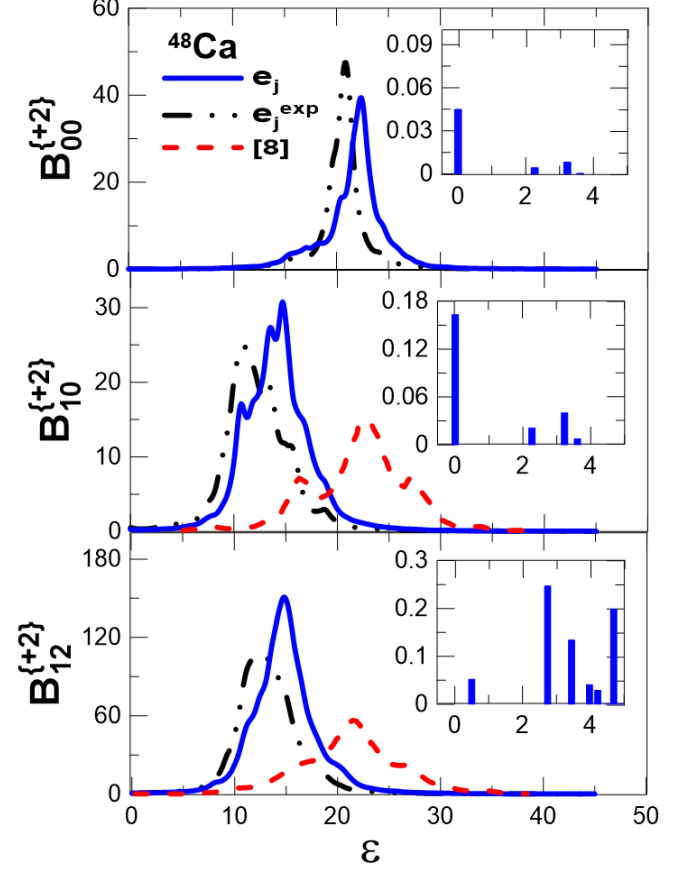


FIG. 6: DCE strength distributions $B_{J\mathcal{J}}^{\{+2\}}$ for the transition $^{48}\text{Ca} \rightarrow ^{48}\text{Ti}$ with spe e_j^{exp} , and e_j^{exp} , and pp strengths T1, as a function of the excitation energy \mathcal{E} in ^{48}Ti . The $B_{J\mathcal{J}}^{\{+2\}}$ are dimensionless, and the energies are in MeV. The SM results, obtained by Shimizu *et al.* [8] with the KB3G interaction, are also shown.

F. Spectral Distributions of Double Charge Exchange Strengths

The DCE strength distributions $B_{J\mathcal{J}_f}^{\{\pm 2\}}$, which are of interest here, are drawn in Figs. 6-8 as a function of the excitation energy \mathcal{E} in final nuclei. We have found that they depend only moderately on the spe spaces, and even less on the pp parameters. To simulate the experimental energy resolution, they were smeared out with Lorentzians of 1 MeV width. Moreover, these figures contain inserts which show the corresponding strengths in the low-lying states of final nuclei.

In the upper panel of Fig. 6 are shown the F distributions $B_{00}^{\{+2\}}$ in ^{48}Ti , exhibiting at around 22 MeV a fairly narrow double giant F resonance, usually called double isobaric analog state (DIAS). In the middle and lower panels of this figure are shown the GT distributions $B_{10}^{\{+2\}}$ and $B_{12}^{\{+2\}}$, respectively, in the same final nucleus, which also exhibit resonant like structure. These dou-

¹⁰ In this case it could be interesting to analyze if the problem can be solved by particle-number projection [55].

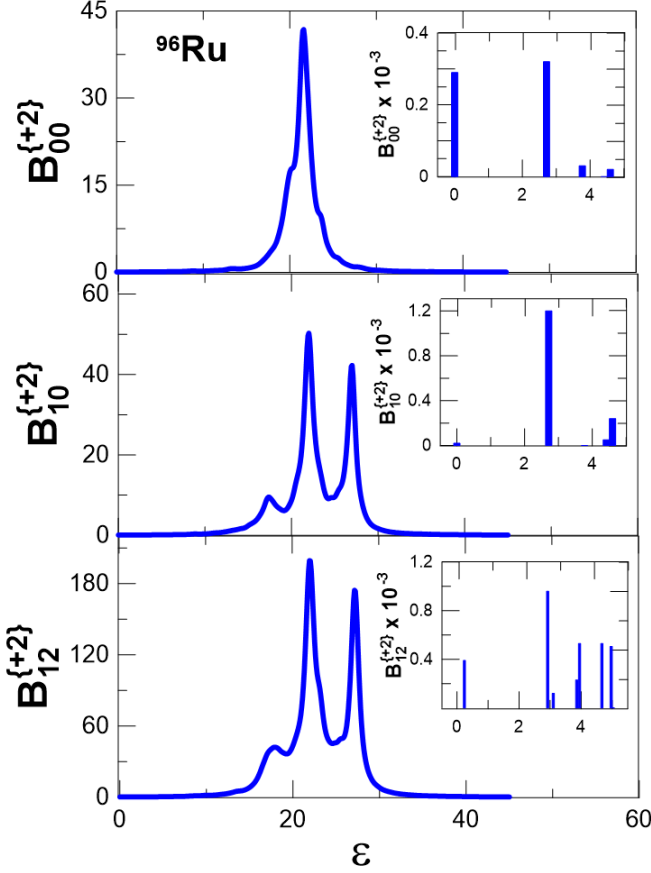


FIG. 7: DCE strength distributions $B_{J\mathcal{J}}^{\{+2\}}$ for the transition $^{96}\text{Ru} \rightarrow ^{96}\text{Pd}$. The $B_{J\mathcal{J}}^{\{+2\}}$ are dimensionless, and the energies are in MeV.

ble GT giant resonances (DGTGR) are much wider than the DIAS and centered around 13 and 14 MeV, respectively. In the KB3G SM calculations of Shimizu *et al.* [8], which are also shown in Fig. 6, these resonances appear at around 20 MeV.

In Figs. 7 and 8 are presented analogous results for the $B_{J\mathcal{J}}^{\{+2\}}$ and $B_{J\mathcal{J}}^{\{-2\}}$ densities in ^{96}Pd and ^{96}Mo final nuclei, respectively. Both are shown because here we are interested in the DBD^+ , where the low-energy behavior of $B_{J\mathcal{J}}^{\{-2\}}$ densities is relevant.

As seen in Fig. 7, the DIAS in ^{96}Pd is located at around 21 MeV, while both $\mathcal{J} = 0^+$ and $\mathcal{J} = 2^+$ DGTGR are at about 23 MeV. These resonances are not directly related to the DBD of ^{96}Ru , but their locations in ^{96}Pd can be searched through heavy ion reactions.

The smallness of $B_{00}^{\{-2\}}$ and its energy distribution, shown in Fig. 8, are fully consistent with the small value of $M_F^{2\nu}(0_1^+)$ in Table III and of $B_{00_1}^{\{-2\}}$ in Table VII. Moreover, the distributions of the $B_{1\mathcal{J}=0,2}^{\{-2\}}$ clearly indicate that the DBD^+ of ^{96}Ru will be very slow.

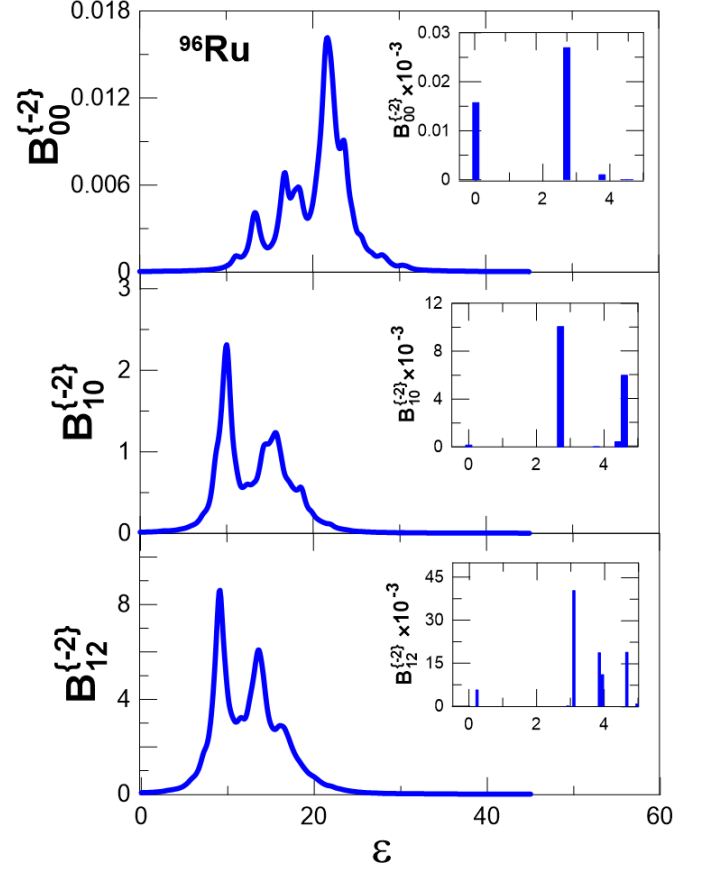


FIG. 8: DCE strength distributions $B_{J\mathcal{J}}^{\{-2\}}$ for the transition $^{96}\text{Ru} \rightarrow ^{96}\text{Mo}$. The $B_{J\mathcal{J}}^{\{-2\}}$ are dimensionless, and the energies are in MeV.

G. Comparison between ground state 2ν -DBD NME and DCE strengths

In the so-called closure approximation, the sum of the intermediate states J_α in (2.1) and (2.9) are taken by closure, after replacing $E_{J_\alpha}^{\{\mp 1\}}$ in (2.3) by some average $\bar{E}_J^{\{\mp 1\}}$ [44].

Thus, except for the constant energy denominator, the ground state DCE densities $B_{J_0}^{\{\pm 2\}}$ are the closure approximations of the squares of the NMEs. In view of this, to know how reasonable the closure approximation is, it may be interesting to compare the behaviors of these two quantities as a function of the pp parameters. As an example, in Fig. 9 are compared the squares of the NMEs $M_F^{2\nu}(0_1^+)$ and $M_{GT}^{2\nu}(0_1^+)$ with $B_{00_1}^{\{+2\}}$, for ^{48}Ca with the spe e_j . The squares of the NMEs are in natural units, while the strengths are dimensionless. The proportionality between these two observables suggests that the closure approximation in the case of ^{48}Ca is reasonable. However, there is no guarantee that this result will be valid in general.

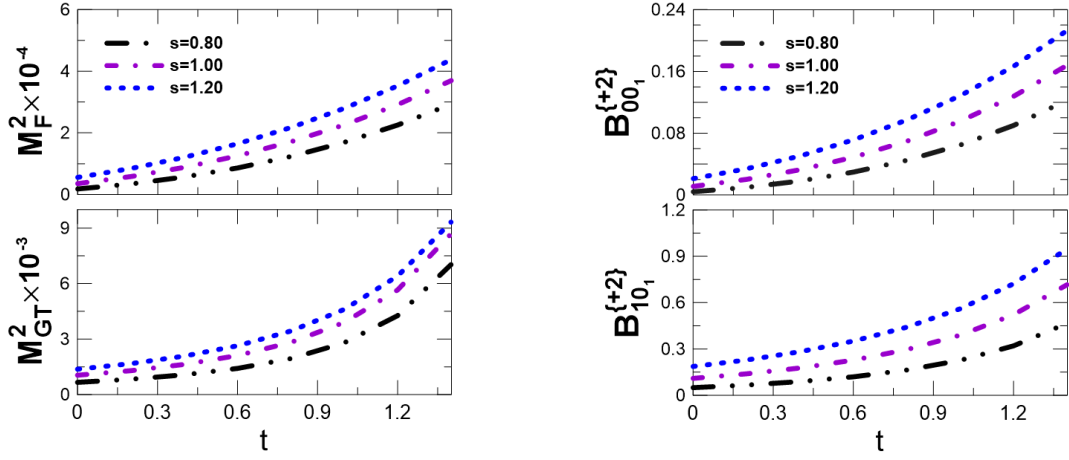


FIG. 9: (Color online) Comparison of $|M_F^{2\nu}(0_1^+)|^2$ and $|M_{GT}^{2\nu}(0_1^+)|^2$ (both in natural units) with $B_{00_1}^{\{+2\}}$ and $B_{10_1}^{\{+2\}}$ (dimensionless), respectively, in ^{48}Ca for the spe e_j .

IV. FINAL REMARKS

We have developed a nuclear structure model that involves (pn,2p2n)-QTDA excitations on the BCS mean-field, which is capable of simultaneously describing the DBD and the DCE transition strengths. So far, this has been done only in the context of SM, where these two problems are generally treated separately, although it is well known that they are intimately related to each other. This is the case, for instance, of ^{48}Ca , where the DBD-s are described in Refs. [17, 41], while the transition strength distributions $B_{J\mathcal{J}}^{\{+2\}}$ and the corresponding total strengths $S_{J\mathcal{J}}^{\{+2\}}$ were evaluated in Refs. [6–8].

The (pn,2p2n)-QTDA model has additional advantages over the standard pn-QRPA model. Namely:

1. Together with the NMEs of the ground state, the NMEs of all the excited states 0^+ and 2^+ are calculated simultaneously. To do the same in the pn-QRPA model, it is necessary to resort to supplementary calculations through several charge-conserving QRPA's, thus introducing several new model parameters.
2. It allows the evaluation of the Q -values for DBDs, which plays a very important role in this type of processes.

The proposed model can be viewed as a natural extension to DCE processes of the pn-QRPA model, originally developed by HS to describe the SCE processes [2]. The first does not include the GSC like the second. But this is not a serious inconvenience since, as we have discussed above, the quenching mechanism is now different.

Our next aim is to evaluate and discuss the 0ν -NMEs (2.12) making use of the replacement (2.11) in our previous work [19]. One expects that the relationship between DCE nuclear reactions and DBD will be more clearly visible at 0ν than at 2ν reactions, due to a lower

dependence on the NME of their energy denominators in the first case.

During the development of the present study, Santopinto *et al.*[56], based on a previous work of Bertulani [57], have reported that, in the low-momentum-transfer limit, the heavy ion $^{40}\text{Ca}(^{18}\text{O}, ^{18}\text{Ne})^{40}\text{Ar}$ cross section behaves as

$$\frac{d\sigma}{d\Omega} \sim \left| \frac{\mathcal{M}_{T \rightarrow T'}^{DGT} \mathcal{M}_{P \rightarrow P'}^{DGT}}{E_P^{GT} + E_T^{GT}} + \frac{\mathcal{M}_{T \rightarrow T'}^{DF} \mathcal{M}_{P \rightarrow P'}^{DF}}{E_P^{DF} + E_T^{DF}} \right|^2,$$

where P and T stand for projectile and target nuclei respectively.

The correspondence with our notation is:

- 1) For the matrix elements ¹¹

$$\begin{aligned} \mathcal{M}_{P \rightarrow P'}^{DGT} &\rightarrow B_{10_1}^{\{+2\}}, & \mathcal{M}_{P \rightarrow P'}^{DF} &\rightarrow B_{00_1}^{\{+2\}}, \\ \mathcal{M}_{T \rightarrow T'}^{DGT} &\rightarrow B_{10_1}^{\{-2\}}, & \mathcal{M}_{T \rightarrow T'}^{DF} &\rightarrow B_{00_1}^{\{+2\}}. \end{aligned}$$

- 2) For the energies (see the denominator in (2.2))

$$\begin{aligned} E_P^{GT} &\rightarrow E_{1_\alpha}^{\{+1\}} - E_{0_+}^{\{0\}}, & E_P^{DF} &\rightarrow E_{0_\alpha}^{\{+1\}} - E_{0_+}^{\{0\}}, \\ E_T^{GT} &\rightarrow E_{1_\alpha}^{\{-1\}} - E_{0_+}^{\{0\}}, & E_T^{DF} &\rightarrow E_{0_\alpha}^{\{-1\}} - E_{0_+}^{\{0\}}. \end{aligned}$$

Therefore, the present model possesses all the necessary ingredients to evaluate the heavy-ion cross section in the low-momentum-transfer limit. Of course, now it is necessary to solve two eigenvalue problems, one for the target nucleus ^{40}Ca , and one for the projectile nucleus ^{18}O .

In summary, we have developed a new model, based on the BCS approach, to describe the double-charge exchange nuclear phenomena $(A, Z) \rightarrow (A, Z \pm 2)$. It is a natural extension of the Halbleib and Sorensen [2] model, aimed to describe the single-charge exchange processes

¹¹ Except for the coupling constants c_{GT} and c_{GT} in Eqs. (11) and (12) respectively.

$(A, Z) \rightarrow (A, Z \pm 1)$. As an example, detailed numerical calculations are presented for the $(A, Z) \rightarrow (A, Z + 2)$ process in $^{48}\text{Ca} \rightarrow ^{48}\text{Ti}$ and the $(A, Z) \rightarrow (A, Z - 2)$ process in $^{96}\text{Ru} \rightarrow ^{96}\text{Mo}$, involving all final 0^+ states and 2^+ states. At the moment we are extending this study in two directions:

1. A throughout evaluation of all 2ν -DBD $^\pm$, together with the associate nuclear reaction strengths will be performed.
2. The 2ν -DBD $^\pm$ formalism developed here will be extended to the 0ν -DBD $^\pm$.

Acknowledgments

This study was financed in part by the Coordenação de Aperfeiçoamento de Pessoal de Nível Superior Brasil (CAPES) Finance Code 001. A.R.S. acknowledges the financial support of FAPESB (Fundação de Amparo à Pesquisa do Estado Bahia) TERMO DE OUTORGA-PIE0013/2016. The authors thank the partial support of UESC (PROPP 00220.1300.1832). We sincerely thank to Wayne Seale for his very careful and judicious reading of the manuscript. We also thank N. Paar for providing us the spe for ^{96}Ru , evaluated within the (DD-ME2) model, and to C. Bertulani and C. Barbero for stimulating comments and discussions.

Appendix: A Toy Model

In order to understand why F DCEsr is not completely satisfied in our model, we resort to a toy model

corresponding to the ^{14}C nucleus and considering the levels $1s_{1/2}$, $1p_{1/2}$, and $1p_{3/2}$, of which the three are totally occupied by neutrons, while only the first two are partially occupied by protons. From (2.14) we have

$$\begin{aligned} S_{00}^{\{-2\}} &= \sum_f B_{00f}^{\{-2\}} \\ &= \sum_f \left| \sum_\alpha \langle 0_f^+ | | \mathcal{O}_f^- | | 0_\alpha^+ \rangle \langle 0_\alpha^+ | | \mathcal{O}_0^- | | 0_i^+ \rangle \right|^2. \end{aligned} \quad (\text{A.1})$$

In the BCS approximation one gets

$$\begin{aligned} B_{001}^{\{-2\}} &= 4u_{1p_{1/2}}^4, \quad B_{002}^{\{-2\}} = 4u_{1s_{1/2}}^2 u_{1p_{1/2}}^2, \\ B_{003}^{\{-2\}} &= 12u_{1s_{1/2}}^2 u_{1p_{1/2}}^2, \quad B_{004}^{\{-2\}} = 4u_{1s_{1/2}}^4, \end{aligned}$$

and

$$S_{00}^{\{-2\}} \equiv S_F^{2\beta^-} = 4 + 8u_{1s_{1/2}}^2 u_{1p_{1/2}}^2, \quad (\text{A.2})$$

since $u_{1s_{1/2}}^2 + u_{1p_{1/2}}^2 = 1$. For instance, with $u_{1s_{1/2}}^2 = 0.95$ and $u_{1p_{1/2}}^2 = 0.05$, one gets $S_{00}^{\{-2\}} = 4.382$, instead of the predicted value $S_{00}^{\{-2\}} = 4$. The result (A.2) also is valid when the residual interaction is switched on. This means that the F DCEsr is fully satisfied only in the particle-hole limit, *i.e.* when one of the protons $1s_{1/2}$, $1p_{1/2}$ levels is totally full or totally empty.

-
- | | |
|--|--|
| <p>[1] F. Krmpotić, <i>Fizika</i> B 14, 139 (2005). http://fizika.hfd.hr/fizika_b/bv05/b14p139.htm</p> <p>[2] J. A. Halbleib and R. A. Sorensen, <i>Nucl. Phys. A</i> 98, 542 (1967). https://doi.org/10.1016/0375-9474(67)90098-X</p> <p>[3] A. S. Barabash, <i>Physics of Elementary Particles and Atomic Nucleus</i> 42, 1183 (2011). http://www1.jinr.ru/Pepan/2011_v42/v-42-4/10_bar.pdf; <i>ibid</i> <i>Nucl. Phys. A</i> 935, 52 (2015). https://doi.org/10.1016/j.nuclphysa.2015.01.001.</p> <p>[4] F. Cappuzzello, M. Cavallaro, C. Agodi, M. Bondi, D. Carbone, A. Cunsolo, and A. Foti, <i>Eur. Phys. J. A</i> 51, 145 (2015). https://doi.org/10.1140/epja/i2015-15145-5</p> <p>[5] D. Carbone <i>et al.</i>, <i>J. Phys. Conf. Ser.</i> 1078 (2018) no.1, 012008. https://iopscience.iop.org/article/10.1088/1742-6596/1078/1/012008</p> <p>[6] H. Sagawa and T. Uesaka, <i>Phys. Rev. C</i> 94, 064325 (2016). https://doi.org/10.1103/PhysRevC.94.064325</p> <p>[7] N. Auerbach, Bui Minh Loc, <i>Phys. Rev. C</i> 98, 064301 (2018). https://doi.org/10.1103/PhysRevC.98.064301</p> <p>[8] N. Shimizu, J. Menéndez, and K. Yako, <i>Phys. Rev. Lett.</i> 120, 142502 (2018). https://doi.org/10.1103/PhysRevLett.120.142502</p> | <p>[9] A. Escuderos, A. Faessler, V. Rodin, F. Simkovic, <i>J. Phys. G</i> 37, 125108 (2010). https://iopscience.iop.org/article/10.1088/0954-3889/37/12/125108</p> <p>[10] J. Suhonen, <i>Phys. Rev. C</i> 86, 024301 (2012). https://doi.org/10.1103/PhysRevC.86.024301</p> <p>[11] D. S. Delion and J. Suhonen, <i>Phys. Rev. C</i> 95, 034330 (2017). https://doi.org/10.1103/PhysRevC.95.034330</p> <p>[12] C. Barbero, F. Krmpotić, and A. Mariano, <i>Phys. Lett. B</i> 345, 192 (1995). https://doi.org/10.1016/0370-2693(94)01592-Z</p> <p>[13] M. Hirsch, K. Muto, T. Oda, H.V. Klapdor-Kleingrothaus, <i>Z. Physik A - Hadrons and Nuclei</i> 347, 151 (1994). https://doi.org/10.1007/BF01292371</p> <p>[14] J. P. Pirinen and J. Suhonen, <i>Phys. Rev. C</i> 91, 054309 (2015). https://doi.org/10.1103/PhysRevC.91.054309</p> <p>[15] H. Li, Z. Ren, <i>Phys. Rev. C</i> 96, 065503 (2017). https://doi.org/10.1103/PhysRevC.96.065503</p> <p>[16] M. Doi and T. Kotani, <i>Prog. Theor. Phys.</i> 87, No. 5, 1207 (1992). https://doi.org/10.1143/ptp/87.5.1207</p> <p>[17] A. A. Raduta, C. M. Raduta, <i>Phys. Lett. B</i> 647, 265 (2007).</p> |
|--|--|

- <http://dx.doi.org/10.1016/j.physletb.2007.02.007>
- [18] A. Shukla, R. Sahu, and V. K. B. Kota, Phys. Rev. C **80**, 057305 (2009). <https://doi.org/10.1103/PhysRevC.80.057305>
 - [19] V. dos S. Ferreira, F. Krmpotić, C. A. Barbero, and A. R. Samana, Phys. Rev. C **96**, 044322 (2017). <https://doi.org/10.1103/PhysRevC.96.044322>
 - [20] P. Vogel, M. Ericson, and J. D. Vergados, Phys. Lett. **B212**, 259 (1988). [https://doi.org/10.1016/0370-2693\(88\)91313-5](https://doi.org/10.1016/0370-2693(88)91313-5)
 - [21] K. Muto, Phys. Lett. B **277**, 13 (1992). [https://doi.org/10.1016/0370-2693\(92\)90948-4](https://doi.org/10.1016/0370-2693(92)90948-4)
 - [22] D. C. Zheng, L. Zamick, and N. Auerbach, Phys. Rev. C **40**, 936 (1989). <https://doi.org/10.1103/PhysRevC.40.936>
 - [23] J. Suhonen, *From Nucleons to Nucleus: Concepts of Microscopic Nuclear Theory* (Springer, Berlin, 2007).
 - [24] M. K. Pal, Y. K. Gambhir, and Ram Raj, Phys. Rev. **155**, 1144 (1966). <https://doi.org/10.1103/PhysRev.155.1144>
 - [25] Ram Raj and M. L. Rustgi, Phys. Rev. **178**, 1556 (1969). <https://doi.org/10.1103/PhysRev.178.1556>
 - [26] M. Baranger, Phys. Rev. **120**, 957 (1960). <https://doi.org/10.1103/PhysRev.120.957>
 - [27] A. Bohr and B.R. Mottelson, *Nuclear Structure, Vol. 1* (W. A. Benjamin, New York, Amsterdam, 78, 1969).
 - [28] J. Kotila and F. Iachello, Phys. Rev. C **87**, 024313 (2013). <https://doi.org/10.1103/PhysRevC.87.024313>
 - [29] S. Stoica, M. Mirea, Front. Phys. **7**, 12 (2019). <https://doi.org/10.3389/fphy.2019.00012>
 - [30] S. Stoica, Chinese Phys. C **43**, No. 6, 064108 (2019). <https://doi.org/10.1088/1674-1137/43/6/064108>
 - [31] K. Nakayama, A. Pio Galeão and F. Krmpotić, Phys. Lett. B **114**, 217 (1982). [https://doi.org/10.1016/0370-2693\(82\)90480-4](https://doi.org/10.1016/0370-2693(82)90480-4)
 - [32] G. E. Brown and Mannque Rho, Nucl. Phys. A **372**, 397 (1981). [https://doi.org/10.1016/0375-9474\(81\)90043-9](https://doi.org/10.1016/0375-9474(81)90043-9); Aage Bohr and Ben R. Mottelson, Phys. Lett. B **100**, 10 (1981). [https://doi.org/10.1016/0370-2693\(81\)90274-4](https://doi.org/10.1016/0370-2693(81)90274-4); H. Castillo and F. Krmpotić, Nucl. Phys. A **469**, 637 (1987). [https://doi.org/10.1016/0375-9474\(87\)90018-2](https://doi.org/10.1016/0375-9474(87)90018-2)
 - [33] S. Yoshida, Y. Utsuno, N. Shimizu, T. Otsuka, Phys. Rev. C **97**, 054321 (2018). <https://doi.org/10.1103/PhysRevC.97.054321>
 - [34] J. Beringer *et al.* (Particle Data Group), Phys. Rev. D **86**, 010001 (2012). <https://doi.org/10.1103/PhysRevD.86.010001>
 - [35] P. Gysbers *et al.*, Nature Physics **15**, 428 (2019). <https://dx.doi.org/10.1038/s41567-019-0450-7>
 - [36] J.T. Suhonen, Front. Phys. **5**, 55 (2017), <https://doi.org/10.3389/fphy.2017.00055>; J. Suhonen, IOP Conf. Series: Journal of Physics: Conf. Series **1056**, 012056 (2018). <https://iopscience.iop.org/article/10.1088/1742-6596/1056/1/012056>
 - [37] C. Conci, V. Klemt and J. Speth, Phys. Lett. B **148**, 405 (1984). [https://doi.org/10.1016/0370-2693\(84\)90727-5](https://doi.org/10.1016/0370-2693(84)90727-5)
 - [38] N. Schwierz, I. Wiedenhover, A. Volya, arXiv:0709.3525 [nucl-th]. <https://arxiv.org/abs/0709.3525v1>
 - [39] M. Kortelainen *et al.*, Phys. Rev. C **89**, 054314 (2014). <https://doi.org/10.1103/PhysRevC.89.054314>
 - [40] F. Krmpotić, A. Samana, and A. Mariano, Phys. Rev. C **71**, 044319 (2005). <https://doi.org/10.1103/PhysRevC.71.044319>
 - [41] M. Horoi, S. Stoica, and B. A. Brown, Phys. Rev. C **75**, 034303 (2007). <https://doi.org/10.1103/PhysRevC.75.034303>
 - [42] M. Horoi, Phys. Rev. C **87**, 014320 (2013). <https://doi.org/10.1103/PhysRevC.87.014320>
 - [43] J. Kotila and F. Iachello, Phys. Rev. C **85**, 034316 (2012). <https://doi.org/10.1103/PhysRevC.85.034316>
 - [44] M. Doi, T. Kotani, H. Nishiura and E. Takasugi, Prog. Theor. Phys. **69**, 602 (1983). <https://doi.org/10.1143/PTP.69.602>
 - [45] R. Almar, O. Civitarese, and F. Krmpotić, Phys. Rev. **C8**, 1518 (1973). <https://doi.org/10.1103/PhysRevC.8.1518>
 - [46] V. Paar, Nucl. Phys. A **211**, 29 (1973). [https://doi.org/10.1016/0375-9474\(73\)90763-X](https://doi.org/10.1016/0375-9474(73)90763-X)
 - [47] N. Paar, private communication.
 - [48] N. Paar, D. Vretenar, T. Marketin, and P. Ring, Phys. Rev. C **77**, 024608 (2008). <https://doi.org/10.1103/PhysRevC.77.024608>
 - [49] A. R. Samana, F. Krmpotić, and C.A. Bertulani, Comput. Phys. Commun. **181**, 1123 (2010). <https://doi.org/10.1016/j.cpc.2010.02.003>
 - [50] M. Hirsch, M. Muto, T. Oda, H.V. Klapdor-Kleingrothaus, Z. Phys. A **347**, 151 (1994). <https://doi.org/10.1007/BF01292371>
 - [51] O. A. Rumyantsev and M. H. Urin, Phys. Lett. B **443**, 51 (1998). [https://doi.org/10.1016/S0370-2693\(98\)01291-X](https://doi.org/10.1016/S0370-2693(98)01291-X)
 - [52] P. K. Raina, A. Shukla, S. Singh, P. K. Rath, and J. G. Hirsch, Eur. Phys. J. A **28**, 27 (2006). <https://doi.org/10.1140/epja/i2005-10280-2>
 - [53] J. Barea, J. Kotila, and F. Iachello, Phys. Rev. C **91**, 034304 (2015). <https://doi.org/10.1103/PhysRevC.91.034304>
 - [54] P. Belli *et al.*, Phys. Rev. C **87**, 034607 (2013). <https://doi.org/10.1103/PhysRevC.87.034607>
 - [55] F. Krmpotić, A. Mariano, T. T. S. Kuo and K. Nakayama, Phys. Lett. B **319**, 393 (1993). [https://doi.org/10.1016/0370-2693\(93\)91740-E](https://doi.org/10.1016/0370-2693(93)91740-E)
 - [56] E. Santopinto, H. García-Tecocoatzi, R.I. Magaña Vsevolodovna, and J. Ferretti (NUMEN Collaboration), Phys. Rev. C **98**, 061601 (2018). <https://doi.org/10.1103/PhysRevC.98.061601>
 - [57] C. A. Bertulani, Nucl. Phys. A **554**, 493 (1993). [https://doi.org/10.1016/0375-9474\(93\)90232-M](https://doi.org/10.1016/0375-9474(93)90232-M)